ABSTRACT

Title of Document:	"Smart" Fluids: Self-Assembled Systems with Viscosity Tunable by Light
	Aimee Marie Ketner, Doctor of Philosophy, 2008
Directed By:	Professor Srinivasa R. Raghavan, Department of Chemical and Biomolecular Engineering

A "smart" fluid is one that undergoes a change in some macroscopic property in response to an external stimulus, such as light or magnetic fields. One class of "smart" fluids is *photorheological (PR) fluids*, which exhibit changes in their rheological or flow properties (such as viscosity) upon irradiation with light at a given wavelength. These PR fluids may be useful in a variety of applications, such as in sensors and microfluidic devices. Currently, the need to synthesize complex photosensitive molecules hampers the widespread use of these fluids. In this dissertation, we are working toward simple classes of PR fluids that require no special synthesis and can thereby be easily replicated in any laboratory from inexpensive chemicals.

In the first part of this study, we report a new aqueous PR fluid that exhibits a 10,000-fold reduction in viscosity upon UV irradiation. The fluid consists of the cationic surfactant, cetyl trimethylammonium bromide (CTAB), and the photoresponsive organic derivative, *trans*-ortho-methoxycinnamic acid (OMCA). Aqueous mixtures of CTAB and OMCA self-assemble into long,

chainlike structures called “wormlike micelles”, and the solution thereby has a very high viscosity. Upon irradiation by UV light (< 400 nm), OMCA undergoes a photoisomerization from its *trans* to its *cis* form, which alters the molecular packing at the micellar interface. The result is to transform the long wormlike micelles into much shorter entities and, in turn, the solution viscosity decreases by more than 4 orders of magnitude. We use small-angle neutron scattering (SANS) to confirm the dramatic reduction in micellar length. Our studies also show how one can tune the magnitude of viscosity reduction in these PR fluids based on the composition of the mixture as well as the duration of the irradiation.

In the second part of this study, we turn our attention to non-aqueous solvents and demonstrate how to make PR fluids in such solvents. The PR effect in these fluids relies on transformations of “reverse” micellar structures formed by a common lipid (lecithin) in conjunction with a stilbene-based photoresponsive additive, 4-hydroxy-4’-nitrostilbene (HNS). Certain mixtures of lecithin/HNS/water in cyclohexane undergo an increase in viscosity (photogelling) upon irradiation with UV light. Interestingly, other compositions of the same mixtures undergo a decrease (photothinning) in viscosity upon irradiation.

Both PR fluids described above provide a one-way (high to low, or low to high) viscosity switch. In the third and final part of this study, we report an aqueous system that provides a true, *reversible* PR fluid, where the viscosity can

be switched from high to low and back using different wavelengths of light. These fluids are based on mixtures of a 22-carbon-tailed cationic surfactant with an azobenzene-based photosensitive molecule, 4-azobenzene carboxylic acid (ACA). The conceptual basis for these fluids is similar to that in our first study, and moreover, these molecules are also inexpensive and available from commercial sources. This opens the door to future investigations on PR fluids from both academic and industrial laboratories and should eventually lead to new applications for this interesting class of responsive materials.

"Smart" Fluids: Self-Assembled Systems with Viscosity Tunable by Light

By

Aimee Marie Ketner

Dissertation submitted to the Faculty of the Graduate School of the
University of Maryland, College Park, in partial fulfillment
of the requirements for the degree of
Doctor of Philosophy
2008

Advisory Committee:
Prof. Srinivasa R. Raghavan, Dept. of Chemical and Biomolecular Engineering, Chair
Prof. Sandra C. Greer, Dept. of Chemical and Biomolecular Engineering
Prof. Panagiotis Dimitrakopoulos, Dept. of Chemical and Biomolecular Engineering
Prof. Daniel E. Falvey, Dept. of Chemistry and Biochemistry
Prof. Donald L. DeVoe, Dept. of Mechanical Engineering

This dissertation is dedicated to my amazing husband, Matthew Ketner, and my parents, Marsha and Edward Dudash, who have provided endless support and encouragement throughout this entire educational process.

ACKNOWLEDGEMENTS

First and most important, I would like to thank my advisor, Dr. Srinivasa Raghavan, for his unlimited encouragement, advice, and support. He provided me with the encouragement to pursue my research further then I ever thought I could. He was a great mentor, providing guidance when needed while also allowing enough space to grow on my own as a researcher. He is full of energy and has this special quality of motivating you even when nothing is going right. I have grown in many ways under his guidance; including improvements in my knowledge and in my writing and presentation skills.

I would like to thank Prof. Daniel E. Falvey and Prof. Donald L. DeVoe for the illuminating discussions and collaborations involving different aspects of my research. I would also like to thank Patrick Elder, an undergraduate student who has been working with me on this project during my first three years.

I am grateful to all of my colleagues in the Complex Fluids and Nanomaterials group: Jae-Ho Lee, Bani Cipriano, Shih-Hung Tung, Hee-Young Lee, Rakesh Kumar, Jennifer Hong, Matt Dowling, Chao Zhu, Oluwatosin Ogunsola, Peter Thomas, Kunshan Sun, George Chacko, Khyati Tiwari, and Gabrielle Galvez. I cherish the friendships I made by joining this great group of people. I would like to thank them for their many insightful and amusing discussions. I would also like to acknowledge all of those whom I have made great friendships with here at UMD; especially Erin Falco, for our countless "long walks" and lunch dates.

I would like to thank my family for all of their support, especially my husband, Matt, for his countless sacrifices, encouragement, love, and support.

Finally, we would like to acknowledge NIST for facilitating the SANS experiments and Dr. Angela Lewandowski and Professor William Bentley for help with the HPLC measurements. This work was partially funded by a seed grant from the Small Smart Systems Center (SSSC) at UMD and a CAREER award from NSF-CTS.

TABLE OF CONTENTS

LIST OF FIGURES

Chapter 1

Introduction and Overview

1.1 Problem Statement

This dissertation is focused on the theme of "smart" responsive materials, and more specifically *photorheological* (PR) fluids.[4] PR fluids are those whose rheological properties (such as viscosity) can be tuned by light irradiation. These fluids can offer a third paradigm for field-driven rheology modulation, following along the path of electrorheological (ER)[5] and magnetorheological (MR)[6] fluids. ER fluids are those that can switch from a liquid to a solid state upon exposure to an electric field, while MR fluids accomplish the same feat when exposed to magnetic fields. ER and MR fluids have been around for more than fifty years, and their ability to switch rheological states has formed the basis for technologies such as dampers, clutches, and valves.[6] Thus, rheology modulation is not just of academic interest, but has the potential to enable new applications.

What advantages could PR fluids offer over ER and MR fluids? It is worth noting that ER and MR fluids are typically dispersions of micron-sized particles in oil, and due to their two-phase nature, they tend to aggregate or settle with time. PR fluids, on the other hand, are likely to be homogeneous, single-phase solutions of photoresponsive molecules, with the molecules assembled into structures at the nanoscale (see Figure 1.1).

Thus, the intrinsic length scale in PR fluids will be much smaller than in ER or MR fluids, and the solutions are likely to be stable for long, periods of time. More importantly, a significant advantage of light over electric or magnetic fields is that light can be directed at a precise spatial location (with a resolution on the order of microns). This property could allow PR fluids to be exploited in microscale or nanoscale devices. In fact, PR fluids could be an enabling technology for microfluidic devices and sensors, and in micro- and nano-electromechanical systems (MEMS and NEMS). Indeed, we can envision constructing a valve or other flow-control device based on PR fluids.

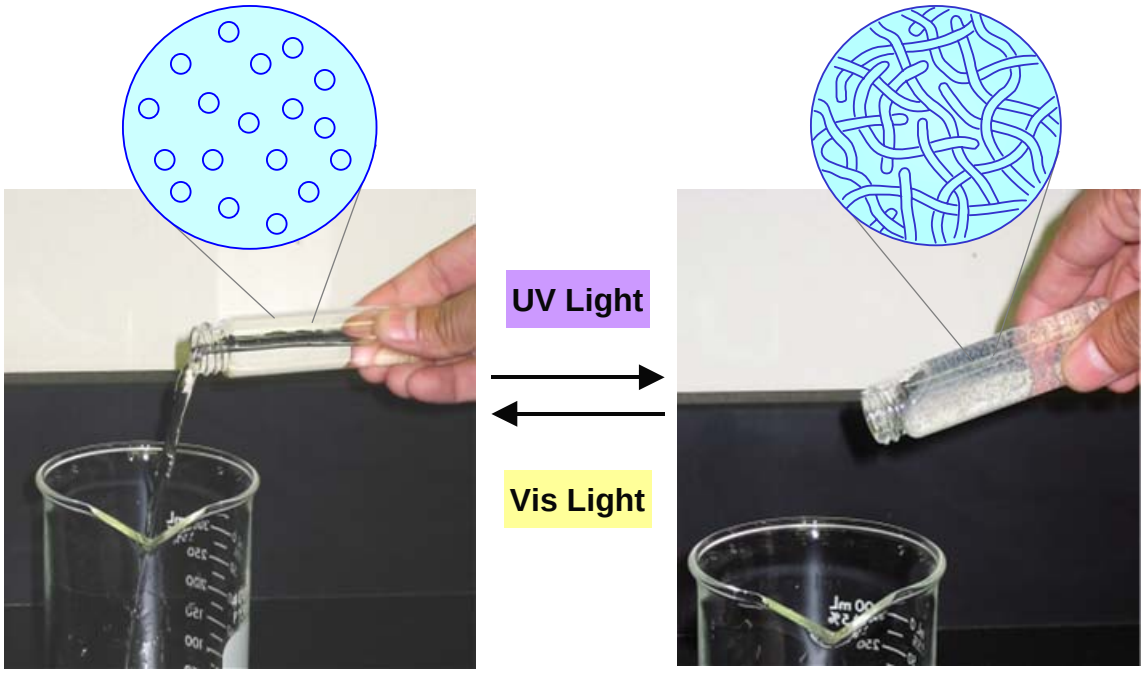

Figure 1.1. Illustration of a PR fluid that can reversibly change its flow properties upon light irradiation. The flow properties correlate with the internal structure in the fluid.

How can one design a PR fluid? What components are needed, and how will it work? A variety of research groups[7-10] have worked on this problem, and the general concept behind most of their attempts is illustrated by Figure 1.1. The idea is to tune the

self-assembly of photoactive molecules in solution using light. Self-assembly refers to the spontaneous aggregation of molecules under a given set of conditions (concentration, temperature, type of solvent). Generally, the type of self-assembled structure formed is sensitive to the geometry (shape) of the precursor molecules, and so the key is to find photoactive molecules that can undergo suitable changes in geometry when illuminated with light. For example, the molecules may initially assemble into a structure that yields a low viscosity (e.g., discrete spheres, Figure 1.1, left). Upon irradiation, however, the change in molecular shape facilitates assembly into a different type of structure that corresponds to a high viscosity (e.g., a network of chains, Figure 1.1, right). Thus, the nanoscale transformation of self-assembled structure is reflected as a dramatic change in viscosity, as shown by the fact that the solution on the left easily pours out of the vial whereas the one on the right is a thick, gel-like material that does not flow out of the vial.

Although the above concept seems straightforward, PR fluids are not widely used at the moment. The chief reason is that the design of PR fluids has so far been tackled as a problem in chemical synthesis. Numerous kinds of complicated photoresponsive molecules, such as, photoresponsive surfactants and polymers bearing azobenzene moieties,[7-10] have been synthesized. Impressive viscosity modulation (even reversible switching of viscosity) has been demonstrated in some cases using such molecules. However, the difficulty in synthesizing these types of molecules has meant that the corresponding PR fluids remain accessible only to a few select research groups. Complicated, labor-intensive synthesis procedures have also made existing PR fluids too expensive for commercial exploitation. As a result, the PR effect has remained of interest

only to a few people in the academic community, and there has been little to no interest from industry. Currently, there is a conspicuous lack of simple, inexpensive approaches to making functional PR fluids, and this provides the motivation for our work.

1.2 Proposed Approach

In this study, we propose to develop new classes of PR fluids that can be made from common, well-known surfactants and photoresponsive additives, which are easily obtained and relatively cheap. The conceptual basis for the proposed PR fluids will rely on transitions between different types of *micellar structures* formed by surfactants in the presence of the photoadditive. A detailed background into surfactant self-assembly is given in Chapter 2. In Chapter 3, we present a class of simple, inexpensive PR fluids that can be made simply by mixing a surfactant and a commercial photoadditive in water. We will demonstrate a dramatic (10,000-fold) reduction in viscosity (photothinning) when these fluids are irradiated with ultraviolet (UV) light. Chapter 4 extends the concepts developed in Chapter 3 to the development of non-aqueous PR fluids in organic solvents. In these systems, the viscosity can be either decreased or increased by irradiation with light (although the effects are not reversible). Finally, in Chapter 5, we present an aqueous *reversible* PR fluid, where the viscosity can be switched from high to low states and back using different wavelengths of light. A variety of techniques, including UV-Vis spectroscopy, rheological measurements, and small-angle neutron scattering (SANS) are used in this study. Details on these techniques are also given in Chapter 2.

From a fundamental standpoint, we seek to understand the behavior of PR fluids (especially the influence of light) at three different length scales:

- **Molecular (Sub-Nano Scales):** What transitions in molecular geometry occur upon irradiation? This is generally probed using UV-Vis spectroscopy. The most frequent type of transition is a *photoisomerization*, such as a transition of a double bond from *trans* to *cis*.

- **Nano-Micro Scales:** What transitions in self-assembled structure (type, size, shape) occur upon irradiation? This is probed using SANS, and it is also possible to use light scattering or cryo-electron microscopy.

- **Macroscale:** Finally, the molecular and structural transitions are reflected as changes in macroscopic (rheological) properties. Thus, we characterize the rheological signature of the fluid before and after irradiation. Ultimately, we seek to correlate the rheology with the self-assembled structure, and in turn with the molecular geometry. Also, we are interested in the kinetics, i.e., how long it takes to switch the rheological properties and the variables that influence this process.

The potential significance of this work is that it could open up the study of PR fluids to an entire range of academic researchers, as well as to researchers in industry. Ultimately, increased research will translate into practical applications for PR fluids in both existing as well as emerging technologies.

Chapter 2

Background

This dissertation is concerned with self-assembled photorheological fluids that are based on surfactants and photoresponsive molecules. In this chapter, we describe the basics of surfactant self-assembly and of photo-induced transitions in molecules. We then briefly describe the techniques we will use to characterize our photorheological fluids, such as rheology, scattering, and UV-Vis spectroscopy.

2.1 Self-Assembly of Amphiphiles

Amphiphiles (also referred to as surfactants, detergents, or lipids) are molecules that contain a hydrophilic portion (head) and a hydrophobic portion (tail). In Figure 2.1, the hydrophilic heads are depicted in blue and the hydrophobic tails in red. When placed in a polar solvent such as water, amphiphiles tend to spontaneously self-assemble into various types of structures. The first type of structures that are formed are spherical micelles, and their formation begins at a threshold concentration of the amphiphile known as the critical micelle concentration or CMC. The process of self-assembly is governed by thermodynamics, i.e., the system minimizes its overall Gibbs free energy in the process. The main driving force for assembly is the hydrophobic effect, i.e., the entropy gain of water molecules when the hydrophobic tails are removed from their midst and buried in the interior of a structure such as a micelle.

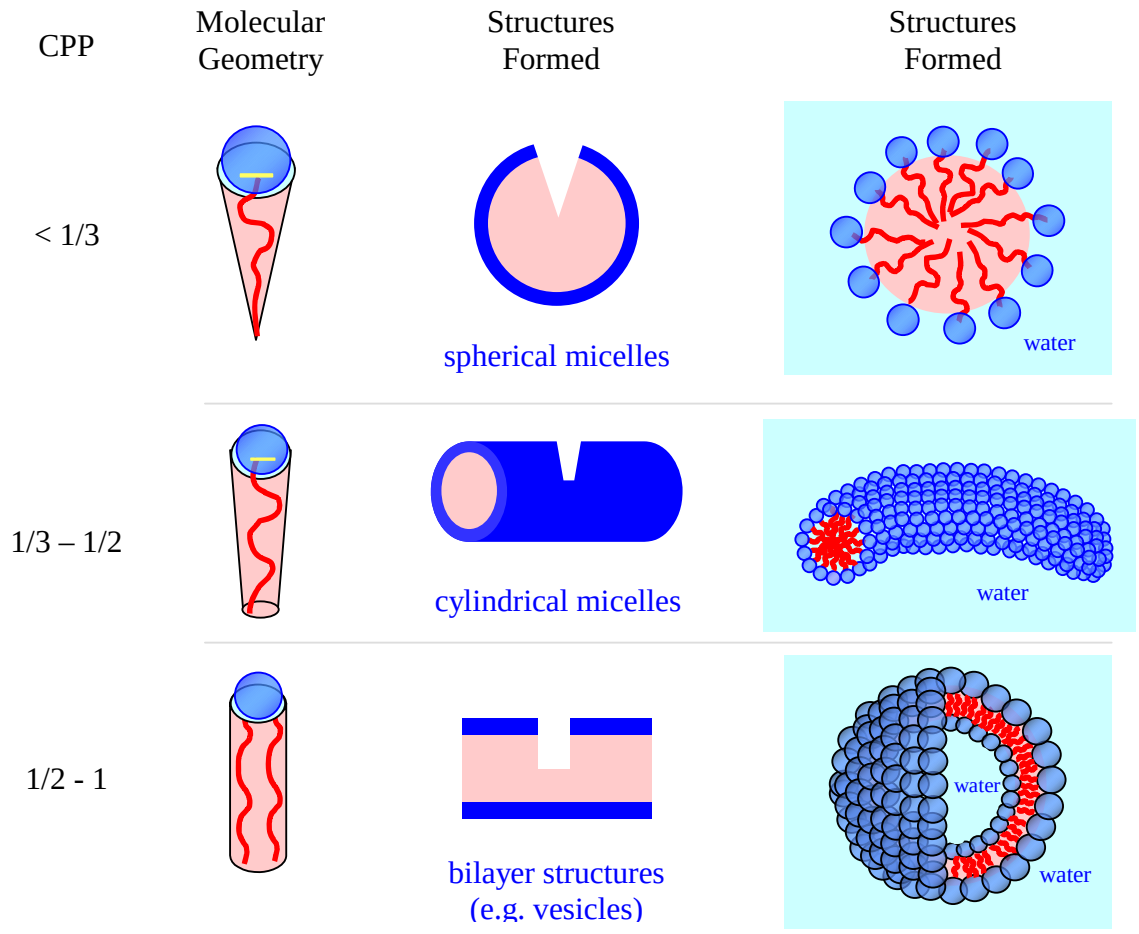

Figure 2.1. Schematics depicting the connection between the geometry of amphiphilic molecules and the structures they form in water. The hydrophilic heads of the amphiphiles are shown in blue and the hydrophobic tails in red. [1]

Figure 2.1 shows that a variety of structures can be assembled from amphiphiles. Micelles can be spherical or cylindrical, and intermediate shapes such as prolate or oblate ellipsoids are also possible. Vesicles are a different kind of structure, formed by the folding of a bilayer or lamellar sheet of amphiphiles. The molecular geometry of the amphiphile generally dictates the type of structure formed by its self-assembly in water.

This correlation is generally quantified by a parameter known as the critical packing parameter (CPP), which is defined as:[11]

$$\mathrm{CPP} = \frac{a_{\mathrm{tail}}}{a_{\mathrm{hg}}} \tag{2.1}$$

where a_{tail} is the average cross-sectional area of the hydrophobic tail and a_{hg} is the effective cross-sectional area of the hydrophilic head.[12-14] The larger the CPP, the greater the curvature of the resulting self-assembled aggregate, as shown by Figure 2.1. In particular, amphiphiles with a CPP = ⅓ (corresponding to a cone shape) form spherical micelles, whereas those with a CPP = ½ (corresponding to a truncated cone geometry) form cylindrical micelles. Finally, amphiphiles that have equal areas of their head and tail and thus a CPP = 1 (cylinder shape) tend to form vesicles and bilayers.

2.2 Wormlike Micelles

As mentioned above, cylindrical micelles form when the CPP of the amphiphile is around 1/2. In some cases, these cylinders can grow into very long and flexible chains, and these are then referred to as wormlike micelles (Figure 2.2). The end-to-end (contour) length of wormlike micelles can be as long as a few microns, i.e., > 1,000 nm (in comparison, spherical micelles have a size of only ca. 5 nm).[15-17] Due to their length, the micelles tend to become entangled in a transient network (Figure 2.2). As a result, the solution becomes highly viscous and *viscoelastic*. The term viscoelastic refers to a combination of viscous (liquid-like) and elastic (solid-like) character in the same sample. The viscoelasticity of the solution is manifested in phenomena such as rod climbing and elastic recoil,[2] as well as in the presence of entrapped bubbles in the sample.

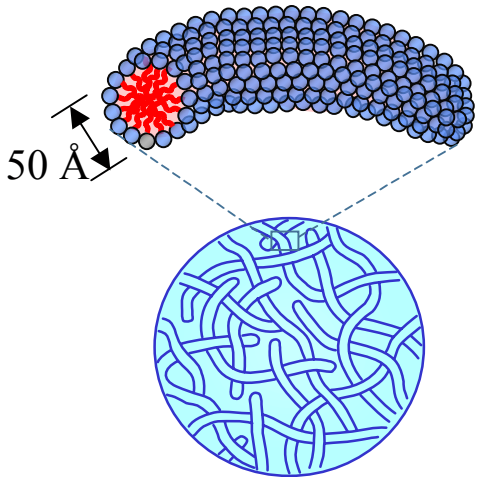

Figure 2.2. Schematic of linear wormlike micelles and their entangled network.[2] The micelles have a locally cylindrical structure, as shown by the close-up.[3]

Another characteristic property of wormlike micelles is their *flow-birefringence*: i.e., when a sample vial is shaken, bright streaks of light are visible under crossed polarizers. Birefringence, also known as double refraction, refers to a difference in refractive indices of a sample along mutually perpendicular directions. It is a characteristic property of anisotropic materials such as liquid crystals.[2] In the case of wormlike micelles, shear induces chains to align along the shear direction, and the sample thus becomes temporarily anisotropic. The birefringence disappears shortly after the shear is stopped.

Wormlike micelles can be formed from several different types of surfactants, but most academic studies have focused on cationic surfactants such as cetyl trimethylammonium bromide (CTAB).[15,18-22] CTAB is an amphiphilic molecule with a 16-carbon length hydrophobic tail and a cationic head group. Generally, for an ionic

surfactant like CTAB, there are strong electrostatic repulsions between the head groups, which cause the effective area of the head to be large. Thus CTAB tends to have a cone-like shape (CPP = ⅓), and accordingly, it will self-assemble into spherical micelles. However, when salt is added to a CTAB solution, the added ions screen the repulsions between the cationic headgroups, reducing the headgroup area, and increasing the CPP from ⅓ to ½. In turn, the spherical micelles are transformed into cylindrical micelles, which then grow uniaxially to become worms.

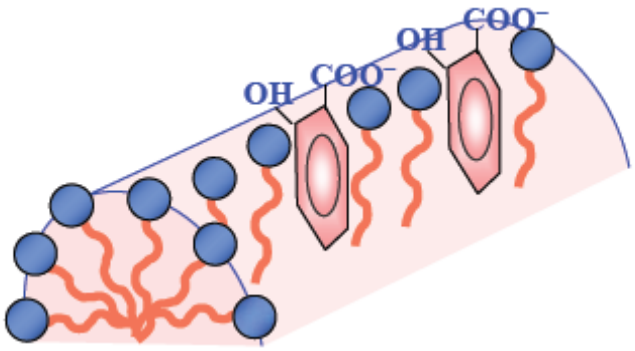

Figure 2.3 Binding of salicylate (o-hydroxy benzoate) counterions to cationic micelles. The aromatic ring is embedded into the hydrophobic interior of the micelle shown in red. The hydrophilic groups (OH and COO^-) protrude out of the micelle, shown in blue. [1]

While all salts can induce the growth of ionic worms, aromatic salts can do so at very low concentrations in comparison with inorganic salts like sodium chloride (NaCl). An example of an effective aromatic salt for cationic surfactants like CTAB is sodium salicylate (NaSal). As shown in Figure 2.3, the salicylate counterions tend to bind strongly to cationic micelles, with their hydrophobic phenyl ring embedded in the hydrophobic interior of the micelle. At the same time, the carboxylate anions from salicylate tend to cancel out the cationic surface charge, thereby reducing the headgroup

repulsion. Consequently, NaSal promotes growth of CTAB worms at very low concentrations, i.e., at NaSal:CTAB molar ratios much less than one. Salts like NaSal are referred to as "binding salts" due to their ability to bind to micelles. In contrast, simple salts like NaCl merely "screen" the electrostatic repulsions between head groups, and must therefore be added at higher concentrations to influence micellar growth. In addition to NaSal, a variety of other aromatic counterions are known to serve as binding salts for cationic surfactants. These include derivatives of tosylate, chlorobenzoate, and hydroxy-naphtalene carboxylate.[17] In Chapter 3, we will show that certain cinnamic acid derivatives can also effectively bind to cationic micelles.

2.3 Reverse Self-Assembly

Molecular self-assembly can also occur in a variety of organic solvents in addition to water. Generally, the organic solvent must be either highly polar or highly non-polar to allow self-assembly of amphiphiles. Self-assembled structures formed in highly non-polar solvents have a reversed geometry compared to those in water. For example, in a reverse micelle (Figure 2.4), the hydrophobic tails (depicted in red) stick out into the oil, while the hydrophilic headgroups (blue) are shielded from the oil phase by being buried in the interior of the micelle. From the viewpoint of molecular geometry, the CPP values for amphiphiles in non-polar solvents need to be greater than 1, which implies that the molecule has a large tail area and a small headgroup area. In the limit of a CPP much larger than 1, the molecules will assemble into reverse spherical micelles, as depicted at the bottom of Figure 2.4. If there is a slight reduction in the tail group area or increase in head group area, the CPP will move closer to 1. This in turn will cause a transition from

reverse spherical micelles to reverse cylindrical micelles, depicted at the top of Figure 2.4. As reverse cylinders grow into very long and flexible chains, they become "reverse wormlike micelles", and these are discussed in the next section.

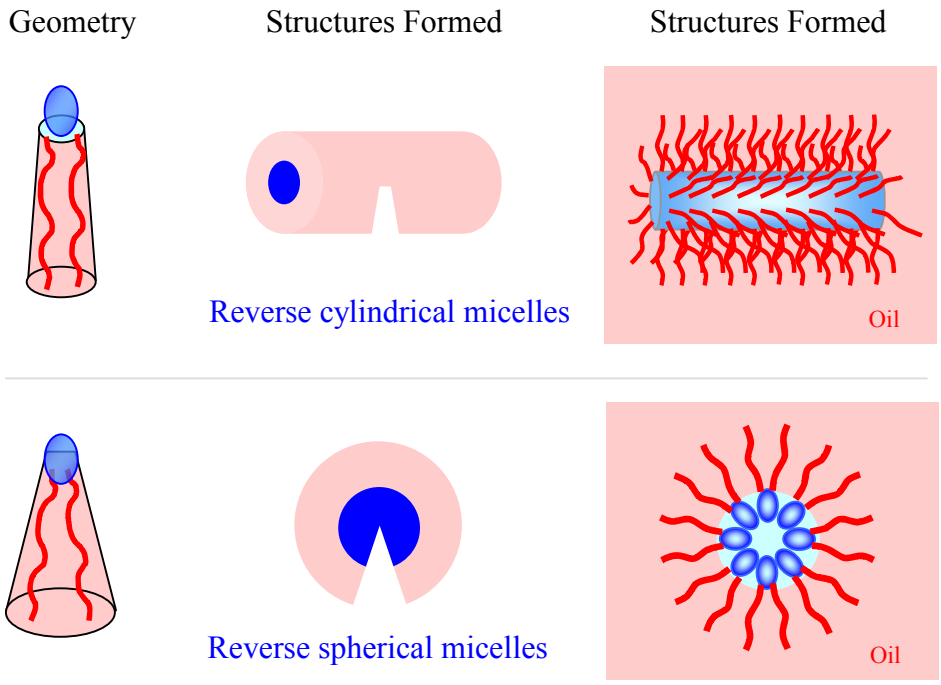

Figure 2.4. Schematics depicting the connection between the geometry of amphiphilic molecules and the structures they form in oil. The hydrophilic heads of the amphiphiles are shown in blue and the hydrophobic tails in red.[3]

2.4 Reverse Wormlike Micelles

Similar to wormlike micelles in water, it is also possible to form reverse wormlike micelles in oil. Figure 2.5 shows the structure of these reverse wormlike micelles; again, note that the hydrophobic tails are directed outward and the hydrophilic heads inward. Only a few amphiphilic formulations have been reported to contain reverse worms,[23-27] most of which are based on the phospholipid, lecithin. Lecithin tends to assemble into

reverse spherical structures when added to non-polar solvents, such as alkanes and cycloalkanes. Upon the addition of a small amount of certain highly polar solvents such as water, the reverse spheres will grow uniaxially into reverse wormlike micelles.[25] The water is believed to sit at the micellar interface and form hydrogen bonds with the phosphate headgroup of the lecithin, thus bridging the lecithin molecules together.[28,29] The hydrogen bonds are thus the driving force for the growth of these reverse wormlike micelles. From a geometric standpoint, the water causes an increase in the CPP by increasing the area of the lecithin headgroup, and this in turn causes the transition from spherical to wormlike reverse micelles.

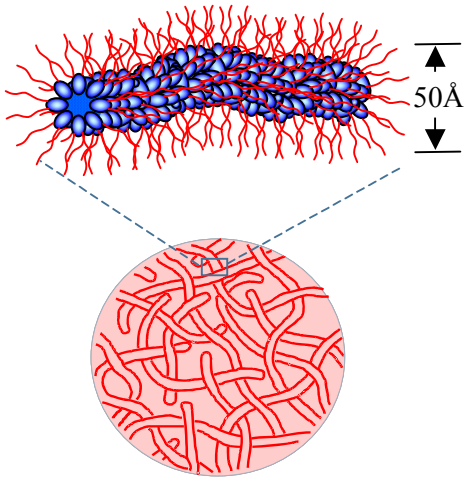

Figure 2.5. Structure of reverse wormlike micelles and their entangled network.[2] The micelles have a locally cylindrical structure, as shown by the close-up.[3]

2.5 Photoresponsive Molecules

Photoresponsive molecules undergo a chemical transformation upon absorption of light at certain wavelengths. One of the main types of photoresponse of interest to us is a

trans to *cis* photoisomerization about double bonds. Such a transformation occurs in molecules such as phenylalkenes, stilbenes, and azobenzenes. Stilbene (IUPAC name: 1,2-diphenylethylene) consists of a C-C double bond with phenyl groups on each carbon (Figure 2.6). This molecule undergoes a *trans* to *cis* photoisomerization under UV light (313 nm).[30] Note that in the *trans* isomer, the phenyl groups are on opposite sides of the double bond, whereas in the *cis* isomer, they are on the same side.

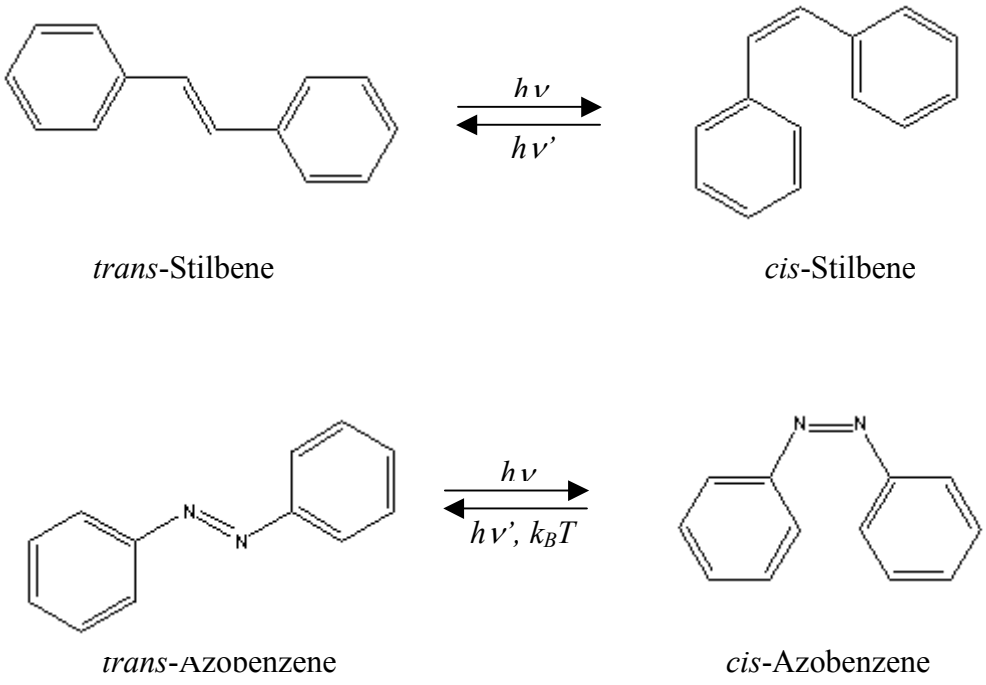

Figure 2.6. UV-induced *trans* to *cis* photoisomerization of stilbene (top) and azobenzene (bottom). The reverse process can be accomplished in the case of azobenzene by irradiating the *cis* form with visible light, or by heat.

Generally, the *trans* to *cis* conversion of stilbene does not occur in the absence of irradiation (ground state) because there is an energy barrier that impedes rotation about the C-C double bond. However, when a *trans*-stilbene molecule in the ground state

absorbs UV light, an electron is promoted from the pi bonding (π) to the pi anti-bonding (π^*) orbital, and the molecule then goes into an excited state. In this excited state, the energy barrier for rotation about the C-C double bond is reduced. Thus, when the molecules fall back to the ground state, they return in equal amounts of *cis*- and *trans*-stilbene. Further UV irradiation converts more of the remaining *trans* isomers to *cis*. At equilibrium (or more precisely, the "photostationary state"), the predominant isomer will be *cis* (e.g., > 80%), but a fraction of *trans* isomers will always remain. In comparison with the *trans*, the *cis* isomer generally absorbs light at shorter wavelengths: for example, the absorption peak is at 254 nm for *cis*-stilbene compared to 313 nm for *trans*-stilbene.[30] In turn, when *cis*-stilbene is irradiated with UV light at 254 nm, it tends to isomerize back to its *trans* form.

Figure 2.6 also illustrates the photoisomerization of azobenzene (IUPAC name: 1,2-diphenyldiazene), which is another well-studied compound. Generally, azobenzene compounds show two absorption peaks: a low-intensity peak in the visible region of the wavelength spectrum, corresponding to an n-π^* excitation (where n is the non-bonding orbital), and a high intensity peak at UV wavelengths, corresponding to a π-π^* excitation.[31] Comparing the *trans* and *cis* isomers of azobenzene, the *trans* has a higher intensity peak in the UV wavelength range, whereas the *cis* has a higher intensity peak at visible wavelengths. This implies that UV light ($330 < \lambda < 380$ nm) can induce a *trans* to *cis* photoisomerization (the photostationary state in this case corresponds to about 80% *cis* and 20% *trans*).[32] In turn, if *cis*-azobenzene is irradiated with visible light ($\lambda > 420$

nm), it isomerizes back to a mostly *trans* state.[32] Interestingly, the *cis* to *trans* transition of azobenzene can also be accomplished by heat instead of light.[32]

Phenylalkenes consist of a *single* phenyl ring attached to a C-C double bond (unlike stilbenes, which have two such phenyl rings). An example is cinnamic acid (IUPAC: 3-phenyl-2-propenoic acid), which has a phenyl ring on one carbon of the double bond and a carboxylic acid moiety on the other carbon. Generally, these cinnamic acid compounds show two peaks in the UV region, a high intensity peak at shorter UV wavelengths, and a lower intensity peak at longer UV wavelengths. The absorption peaks of the *trans* and *cis* isomers fall within a few nm of each other (280 and 283 nm for *cis*- and *trans*-cinnamic acid respectively), but the peak is much higher for the *trans* isomer. UV irradiation can thus induce a *trans* to *cis* isomerization of cinnamic acid, but the reverse transition (i.e., *cis* to *trans*) cannot be accomplished with light.[33] In Chapter 3, we will use a cinnamic acid derivative, viz. ortho-methoxy cinnamic acid (OMCA) that also undergoes a *trans* to *cis* isomerization when exposed to UV light. Again, this isomerization cannot be reversed using light at a different wavelength.

2.6 Characterization Technique – I: Rheology

Rheology is defined as the study of the deformation and flow in materials.[34,35] Rheological measurements are useful in characterizing complex fluids and soft materials: they help to correlate the microstructure to the macroscopic flow properties of the material. Typically, rheological measurements are performed under steady or dynamic shear. Under steady shear, the instrument (rheometer) subjects the sample to a constant

shear rate $\dot{\gamma}$ by applying a continuous rotation to the sample at a fixed rate. The sample response is measured as a shear stress σ and the (apparent) viscosity η is calculated as the ratio of the shear stress to shear rate ($\eta = \sigma / \dot{\gamma}$). A plot of η vs. shear rate is called the flow curve of the material.[2] Many fluids and soft materials have a regime in their flow curve at low shear rates where the viscosity is *independent* of shear rate. The viscosity in this "Newtonian plateau region" is called the zero-shear viscosity η_0, and it corresponds to the viscosity of the sample in the limit of $\dot{\gamma} \to 0$.[35]

Rheological experiments can also be conducted in dynamic or oscillatory shear, where the instrument subjects the sample to a sinusoidal strain $\gamma = \gamma_0 \sin(\omega t)$. Here γ_0 is the strain-amplitude (i.e. the maximum applied deformation) and ω is the frequency of the oscillations. The sample response will be in the form of a sinusoidal stress $\sigma = \sigma_0 \sin(\omega t + \delta)$, which is shifted by a phase angle δ relative to the strain waveform. The stress can be decomposed into two components using trigonometric identities, the first being in-phase with the sinusoidal strain, and the second being out-of-phase by 90°:

$$\sigma = \gamma_0 \left[G'(\omega) \sin\left(\omega t\right) + G''(\omega) \cos\left(\omega t\right) \right] \tag{2.2}$$

Here G' is the **Elastic** or **Storage Modulus** and G'' is the **Viscous** or **Loss Modulus**. The dynamic experiment ultimately yields plots of G' and G'' as functions of ω (usually plotted on a double-log scale), which are collectively called the frequency spectrum of the material. This type of plot is useful because it shows how the viscoelasticity of the material varies with time scales, which in turn is a signature of the microstructure.[34]

The physical interpretations of G' and G'' are as follows. The elastic modulus G' is obtained from the in-phase component of the stress, and provides information about the elastic nature of the material. G' is also called the storage modulus since elastic behavior implies the storage of deformational energy. The viscous modulus G'' is extracted from the out-of-phase component of the stress, and it characterizes the viscous nature of the material. G'' is also known as the loss modulus since viscous deformation results in the dissipation of energy. G' and G'' are meaningful only if the dynamic rheological measurements are taken in the "linear viscoelastic" or LVE regime.[35] The LVE regime corresponds to low imposed strains, such that the stress response is linearly proportional to the strain. In that case, G' and G'' will be independent of strain amplitude and will only be functions of the oscillatory frequency ω – in other words, the moduli will be true material properties.

An important advantage of dynamic rheology is that it enables the characterization of the material's microstructure without disrupting it. Since only small-amplitude strains are used (within the LVE regime), the net deformation imposed on the sample is minimal. Thus, the linear viscoelastic moduli reflect the microstructure present in the sample at rest.[34] In contrast, steady-shear rheology measures material properties under continuous flow conditions, which correspond to relatively large deformations. Therefore, dynamic rheological parameters can be correlated with static microstructures and steady-shear rheological measurements correspond to flow-induced changes in the microstructure.

2.7 Characterization Technique – II: SANS

Scattering techniques are invaluable for probing the structures of materials on the micro- and nanometer scale.[36] The underlying principle behind these techniques is that the intensity of elastically scattered radiation from a structured fluid sample is a function of the size, shape, and orientation of the "particles" present in the sample. For this study, small-angle neutron scattering (SANS) is the technique of choice because the contrast between the solvent and the "particles" can easily be achieved by switching the hydrogen in the solvent molecules with deuterium, for example using D_2O instead of H_2O. Also, SANS is useful in probing size scales on the order of a few nm because, the incident radiation in SANS is composed of neutrons having a wavelength of ~ 6 Å. SANS experiments require a nuclear reactor to generate neutrons and we are fortunate to have one of the premier facilities for SANS nearby at the National Institute of Standards and Technology (NIST) in Gaithersburg, MD.

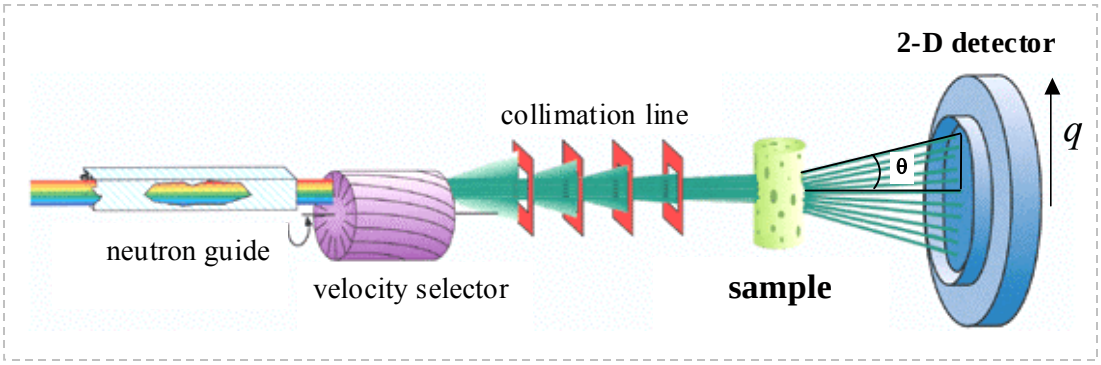

Figure 2.7. Schematic of a SANS experiment (adapted from www.gkss.de).

Figure 2.7 illustrates the basic geometry of a SANS experiment. A nuclear reactor emits neutrons, which then pass through a velocity selector set for a particular

wavelength and wavelength spread. These neutrons then pass through several collimating lenses and into the sample placed in the sample chamber. Finally, a 2-D detector collects the neutrons scattered by the sample. Based on calibration standards, the collected 2-D data are corrected and placed on an absolute scale. These data are then spherically averaged to give a plot of the scattered intensity I vs. wave vector q. The wave vector is defined as:[36]

$$q = \frac{4\pi}{\lambda} \sin\left(\frac{\theta}{2}\right) \tag{2.3}$$

Here, λ is the wavelength of the incident radiation and θ is the scattering angle. q can be considered an inverse length scale, with high q corresponding to small structures, and low q to large structures in the sample.

For a structured fluid containing n_p particles per unit volume, the intensity $I(q)$ can be expressed as follows:[36]

$$I(q) = n_p \cdot P(q) \cdot S(q) \tag{2.4}$$

where $P(q)$ is referred to as the form factor and $S(q)$ as the structure factor. $S(q)$ is the scattering that arises from *interparticle* interactions and thus reflects the spatial arrangement of the particles in the sample. $P(q)$ is the scattering that arises from *intraparticle* interferences, and thus is a function of the particle size and shape. When the particles are in dilute solution (i.e., n_p is small), the interparticle interactions become negligible and therefore the structure factor $S(q) \rightarrow 1$. The SANS intensity $I(q)$ can then be modeled purely in terms of the form factor $P(q)$, i.e., the sizes and shapes of the

particles. The form factors for several different particle geometries have been developed, which can be fit to the data to extract structural information about the particles.

Given below are the form factors for two different micellar shapes: ellipsoids and rigid cylinders. We will use these equations to model the SANS data in Chapter 3. In each of these equations, $\Delta\rho$ is the difference in the scattering length density between the micelle and solvent, and $(\Delta\rho)^2$ is thus a measure of the scattering contrast.

Ellipsoids: The form factor *P(q)* for ellipsoids of revolutions with minor and major axis R_a and R_b is given by:[37,38]

$$P(q) = \left(\Delta\rho\right)^2 \left(\tfrac{4}{3}\pi R_a R_b^2\right)^2 \int_0^1 \left[3\frac{(\sin z - z\cos z)}{z^3}\right]^2 d\mu \tag{2.5}$$

where $z = q\sqrt{\mu^2 R_b^2 + R_a^2\left(1-\mu^2\right)}$. Here, μ is the cosine of the angle between the scattering vector q and the symmetry axis of the ellipsoid.

Cylinders: The form factor $P(q)$ for rigid cylindrical rods of radius R and length L is given by:[37,38]

$$P(q) = \left(\Delta\rho\right)^2 \left(\pi R^2 L\right)^2 \int_0^{\pi/2} \left[F(q,\alpha)\right]^2 \sin\alpha \, d\alpha \tag{2.6}$$

where,
$$F(q,\alpha) = \frac{J_1\left(qR\sin\alpha\right)}{\left(qR\sin\alpha\right)} \cdot \frac{\sin\left(qL\cos\alpha/2\right)}{\left(qL\cos\alpha/2\right)} \tag{2.7}$$

Here α is the angle between the cylinder axis and the scattering vector q and $J_1(x)$ is the first-order Bessel function of the first kind.

2.8 Characterization Technique – III: UV-Vis Spectroscopy

UV-Vis absorption spectroscopy is an analytical technique used to study molecules that adsorb radiation in the ultraviolet (200 to 400 nm) and visible (400 to 800 nm) regions of the electromagnetic radiation spectrum.[33] Generally, when a molecule absorbs radiation, the energy gained is proportional to the energy of the incident photons. In the UV-Vis range, the absorbed energy typically acts to move electrons into higher energy levels.[33] A given molecule does not absorb energy continuously throughout a spectral range because the absorbed energy is quantized; therefore, the molecule will absorb at the wavelength that provides the exact amount of energy necessary to promote it to the next higher energy level.[33] Therefore, each compound will have a unique UV-Vis absorption spectrum. UV-Vis can thus serve as a convenient analytical technique for a variety of compounds, especially those that have an aromatic group.

A typical UV-Vis experiment involves placing a solution containing a low concentration of solute (10^{-5} to 10^{-2} M) in a cuvette, which is then placed in the sample cell of a UV-Vis spectrometer. Light is broken down into its component wavelengths in the spectrometer and passed through the sample. The absorption intensity is measured for each wavelength and a UV-Vis spectrum (plot of absorbance vs. wavelength) is produced for the sample. UV-Vis spectroscopy can be used as a quantitative analytical method to determine the concentration of a solute in solution. This can be done using the Beer-Lambert law:[33]

$$A = \varepsilon \cdot c \cdot \ell \tag{2.8}$$

where A is the measured absorbance at a particular wavelength, c is the concentration of the solute in mol/L, ℓ is the path length of the sample, and ε is the molar extinction coefficient or molar absorptivity at that wavelength. UV-Vis spectroscopy has an important role to play in the study of photoresponsive systems. For example, different photoisomers have different UV-Vis spectra, enabling their easy identification. Also, the peak absorption wavelength is generally the wavelength at which the compound is irradiated to induce a phototransition.

Chapter 3

Photothinning Aqueous Fluids

The results presented in this chapter have been published in the following journal article: Aimee M. Ketner, Rakesh Kumar, Tanner S. Davies, Patrick W. Elder, and Srinivasa R. Raghavan, "*A Simple Class of Photorheological Fluids: Surfactant Solutions with Viscosity Tunable by Light*." J. Am. Chem. Soc. 129, 1553-1559 (**2007**).

3.1 Introduction

In Chapter 1, we described the motivation for our work, which is to discover simple routes to photorheological (PR) fluids that do not require elaborate synthesis of complex molecules. In this chapter, we report a new class of PR fluids that is based entirely on simple, inexpensive chemicals available to any laboratory. The fluids are composed of the cationic surfactant, cetyl trimethylammonium bromide (CTAB), together with a cinnamic acid derivative, i.e., *trans*-*ortho*-methoxycinnamic acid (OMCA). We show that CTAB/OMCA mixtures form wormlike micelles[15,39,40] in aqueous solution and that, upon irradiation by UV light (< 400 nm), the viscosities of these solutions can be made to drop by more than 4 orders of magnitude. The basis for this viscosity change is the *trans* to *cis* photoisomerization of the double bond in OMCA (Figure 3.1). The resultant change in the geometry of OMCA alters the molecular packing of the CTAB/OMCA complex, leading to a drastic reduction in the length of the wormlike micelles (Figure 3.1). In turn, the sample is transformed from a highly

viscoelastic, gel-like fluid to a thin, runny fluid with a viscosity close to that of water. Confirmation of the above microstructural hypothesis is provided by data from SANS.

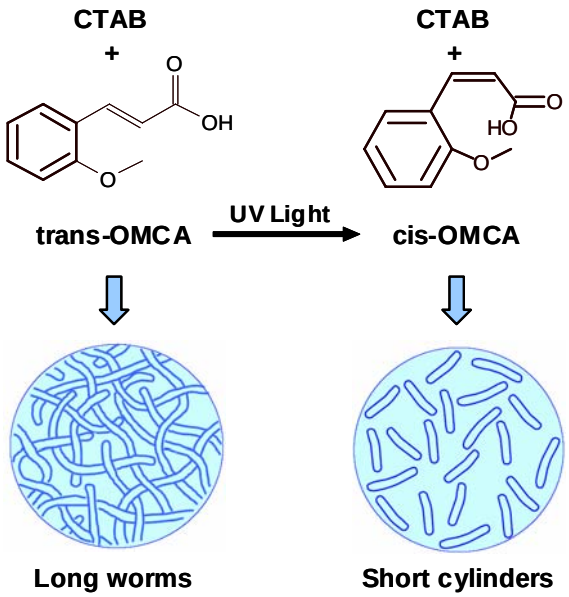

Figure 3.1. Schematic behavior of photoresponsive (PR) fluids consisting of CTAB and OMCA. When OMCA is in its *trans* from, its mixture with CTAB gives rise to long, entangled wormlike micelles. Upon UV irradiation, *trans*-OMCA gets photoisomerized to *cis*-OMCA, and the corresponding change in molecular geometry causes a drastic reduction in micellar length.

It is useful to place our study in the context of earlier studies with PR fluids. Mixtures of surfactant micelles and photosensitive additives have been investigated for a long time, following the pioneering work of Wolff and co-workers (indeed, to our knowledge, it was Wolff who coined the term "photorheological fluid").[4,41-43] Wolff's studies mainly focused on anthracene and stilbene derivatives added to cationic surfactants like CTAB. It is notable that Wolff's studies were all done with simple systems based on conventional surfactants, in much the same spirit as the present study. However, the viscosity changes induced by light in Wolff's samples were rather modest

(factors of 2 to 10).[4,43] Here, we will show that much larger viscosity changes (factors of 1000 to 10,000) can be achieved in CTAB/OMCA mixtures.

Following Wolff's studies, the design of PR fluids was approached by several research groups that were adept in synthetic organic chemistry. These groups focused on making PR fluids using photoresponsive surfactants and/or polymers. For example, Hatton *et al*.[8] worked with a cationic surfactant containing an azobenzene moiety, *viz*. azobenzene trimethylammonium bromide (azoTAB). They mixed azoTAB with a hydrophobically modified polymer to form a viscous solution. Upon UV irradiation, azoTAB isomerized from *trans* to *cis*, which led to a 100-fold drop in viscosity. Moreover, under visible light, the *cis* forms reverted to *trans*, and the viscosity increased back to 50% of its original value. An azoTAB-like surfactant was also used by Sakai *et al*.,[9] who combined it with CTAB and sodium salicylate to produce wormlike micelles. Again, the authors showed that a reversible change in viscosity by a factor of 1000 was possible, with the viscosity decreasing upon UV irradiation and reverting to close to its original value upon irradiation by visible light.

Azobenzene-modified water-soluble polymers have also been used to produce PR fluids. Tribet *et al*.[10] synthesized polyacrylate-based polymers containing octadecyl and azobenzene hydrophobes tethered at random points off the backbone. They added an amphiphilic protein to this polymer to increase the solution viscosity. Under UV light, the *trans* to *cis* isomerization of the azobenzene groups lead to a 40-fold decrease in viscosity, while subsequent irradiation with visible light restored the original viscosity.

Finally, an azobenzene-modified cholesterol has been used as an organogelator to produce non-aqueous PR fluids. Shinkai *et al*.[44] showed that adding this molecule to organic solvents gave rise to stable gels due to the stacking of the cholesterol. Upon UV irradiation, the gel was disrupted due to the isomerization of the azo moiety. Subsequent irradiation with visible light caused the gel to reform.

To summarize, while the underlying principle behind PR fluids has been demonstrated, most of the current systems are lacking in one respect or the other, which explains the lack of commercial applications for these fluids. On the one hand, Wolff and co-workers studied very simple systems, but the magnitude of the PR effect they obtained was weak. On the other hand, impressive photoresponses and even reversible viscosity changes have been demonstrated with fluids based on photoresponsive surfactants or polymers, but those systems are too complicated and costly for widespread use. We believe the CTAB/OMCA system described here can address many of these earlier deficiencies. The composition is simple and the fluids are easy to prepare – yet, we will demonstrate that the PR effect is dramatic (1000-fold changes in viscosity). We hope that this work will stimulate studies into new designs for PR fluids as well as applications for these fluids in microscale devices. From a fundamental standpoint, the principle behind our results, viz., the ability to fine-tune micellar assembly by exploiting molecular geometry, should be applicable to a wide range of organic additives.

3.2 Experimental Section

Materials. CTAB was purchased from Sigma-Aldrich and was greater than 98% in purity. OMCA in its *trans* form was purchased from Acros Chemicals, while the *cis* form was purchased from TCI America, and each compound was greater than 98% in purity. All chemicals were used as received. Ultrapure deionized water from a Millipore water purification system was used in preparing samples for rheological characterization, while D_2O (99.95% deuterated, from Cambridge Isotopes) was used for the SANS studies. Solutions containing OMCA were prepared with a slight excess of base (NaOH), and CTAB was then added to these solutions to reach the final composition. Samples were stirred continuously under mild heat until they became homogeneous. The solutions were then left to equilibrate overnight at room temperature before any experiments were conducted. The pH in the samples was between 9 and 11.

Sample Response Before and After UV Irradiation. CTAB/OMCA samples were irradiated with UV light from an Oriel 200 W mercury arc lamp. A dichroic beam turner with a mirror reflectance range of 280 to 400 nm was used to access the UV range of the emitted light. Samples (5 mL) were placed in a Petri dish with a quartz cover, and irradiation was done for a specific duration under stirring. Due to the nature of the OMCA spectra, irradiated samples did not undergo any changes when stored under ambient conditions, which made it easy to conduct subsequent tests using appropriate techniques such as UV-Vis spectroscopy, HPLC, rheology, and SANS. UV-Vis

spectroscopy before and after irradiation was carried out using a Varian Cary 50 spectrophotometer.

HPLC Studies. The irradiated solutions were analyzed using high-performance liquid chromatography HPLC. The column used was a Waters Spherisorb with 5 μm ODS2, 4.6 mm x 250 mm C18. A flow rate of 0.8 mL/min was used, and the eluting solvent was 15% ethanol and 85% water. The solution components were detected using UV absorption (Dynamax absorbance detector model UV-D II) at 225 and 254 nm. These parameters were based on those of a study of similar molecules by Imae *et al*.[45] HPLC chromatograms were obtained on CTAB/OMCA solutions before and after irradiation.

Rheological Studies. Steady and dynamic rheological experiments were performed on an AR2000 stress controlled rheometer (TA Instruments, Newark, DE). Samples were run at 25°C on a cone-and-plate geometry (40-mm diameter, 2° cone angle) or a couette geometry (rotor of radius 14 mm and height 42 mm, and cup of radius 15 mm). Dynamic frequency spectra were obtained in the linear viscoelastic regime of each sample, as determined by dynamic stress-sweep experiments.

Solubility Studies. The solubility of OMCA isomers in water at 25°C was determined as follows, much like in an earlier study.[46] An excess of the organic derivative was added to deionized water, and the solution was stirred under mild heat for 1 day, followed by equilibration at room temperature for two more days. A sample of this solution in a 1 mm cuvette was placed in the holder of the UV-Vis spectrophotometer, maintained at 25°C.

The sample was left undisturbed for 1 h to allow any undissolved material to settle to the bottom of the cuvette. The absorbance was then measured and converted to a concentration value using the absorptivity determined from a calibration curve. The same procedure was repeated for each of the OMCA isomers.

Small Angle Neutron Scattering (SANS). SANS measurements were made on the NG-7 (30 m) beamline at NIST in Gaithersburg, MD. Neutrons with a wavelength of 6 Å were selected. Two sample-detector distances of 1.33 and 13.2 m were used to probe a wide range of wave vectors from 0.004 to 0.4 $Å^{-1}$. Samples were studied in 2 mm quartz cells at 25°C. The scattering spectra were corrected and placed on an absolute scale using calibration standards provided by NIST. The data are shown for the radially averaged intensity I as a function of the wave vector q (see eq 2.3).

SANS Modeling. For dilute solutions of noninteracting scatterers, the SANS intensity $I(q)$ can be modeled purely in terms of the form factor $P(q)$ of the scatterers (i.e., the structure factor $S(q) \rightarrow 1$ in such cases). In this study, we use form factor models for two different micellar shapes: ellipsoids and rigid cylinders.[37] The corresponding equations are given in Section 2.5 (eq 2.5 to 2.7). The models were implemented using software modules supplied by NIST within the Igor Pro™ program.

3.3 Results and Discussion

We first present UV-Vis spectra for *trans* and *cis*-OMCA in Figure 3.2. These experiments were done with aqueous solutions containing 1 mM of the corresponding derivatives along with a slight excess of base. Figure 3.2 shows that the *trans* form has absorbance peaks at 270 and 312 nm, whereas the peaks for the *cis* form occur at 254 and 293 nm. Note that the *trans* form has much higher absorbances than the *cis* form over the entire UV range. Thus, irradiation of the *trans* derivative with UV light will cause the molecule to absorb light, and this, in turn, can trigger a photoisomerization to its *cis* state. As discussed in Section 2.3, a similar transition does occur for other phenylalkenes, such as cinnamic acid. To test whether photoisomerization occurs for OMCA, we irradiated the *trans*-OMCA solution with UV light (< 400 nm) and recorded UV-Vis spectra after irradiation – these are also shown in Figure 3.2.

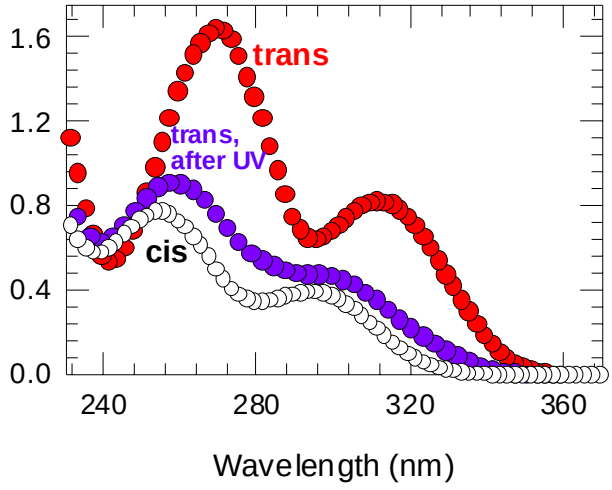

Figure 3.2. UV-Vis spectra of *trans*-OMCA before irradiation, *trans*-OMCA after UV irradiation, and *cis*-OMCA. Each sample is an aqueous solution containing 1 mM of the corresponding additive. The drop in absorbance and blue shift in the *trans*-OMCA curve after UV irradiation indicate that the molecule has been photoisomerized to its *cis* form.

Figure 3.2 shows that there is a blue shift (i.e., to lower wavelengths) in the UV spectrum of *trans*-OMCA upon UV irradiation. That is, the peaks shift from 270 and 312 nm before irradiation to 257 and 300 nm after irradiation, the peak heights are also significantly reduced. This blue shift is indicative of a *trans* to *cis* photoisomerization. The irradiated sample corresponds to a photostationary equilibrium of about 83% *cis* isomers: i.e., its spectrum can be obtained by superposing those for pure *cis* and *trans* in a ratio of 83:17. Interestingly, just 1 min of UV irradiation is enough to cause the transition, and no further changes in the spectrum occur with longer irradiation times.

We now consider the effects of UV irradiation on mixtures of OMCA with the cationic surfactant, CTAB. Henceforth, the abbreviation OMCA will be used to refer to its *trans* form, which is the common, commercially available isomer. (On the other hand, *cis*-OMCA will be specifically denoted as such). Incidentally, the presence of CTAB has no effect on the UV spectra of OMCA and thereby on the UV-induced *trans* to *cis* photoisomerization. Our initial studies with the CTAB/OMCA mixtures showed that these could form highly viscous and viscoelastic solutions. For example, Figure 3.3 shows photographs of a sample containing 60 mM CTAB and 50 mM OMCA. This sample is viscous enough that it does not flow readily out of a tilted vial (Figure 3.3A). Also, when bubbles are introduced by shaking the vial, they remain trapped in the fluid for long periods of time. The sample also shows flow-birefringence; i.e., when viewed under crossed polarizers, streaks of light appear upon gently shaking or tapping the vial (Figure 3.3A).[40] Taken together, the viscoelasticity and flow-birefringence suggest the presence of long wormlike micelles (Section 2.2) in the CTAB/OMCA sample.[40,46] On

the other hand, CTAB/*cis*-OMCA mixtures are visually quite different. Those samples are low-viscosity, water-like solutions that do not show any flow birefringence (viscosity data for these mixtures will be presented later in Figure 3.7).

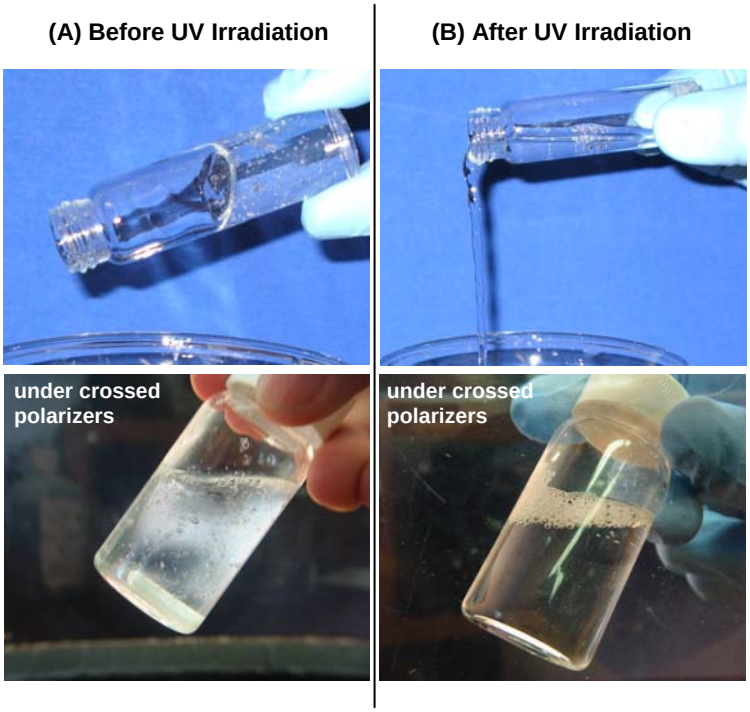

Figure 3.3. Photographs of a 60 mM CTAB + 50 mM OMCA sample (A) before and (B) after UV irradiation. (A) Initially, OMCA is in its *trans* form, and the sample is highly viscoelastic due to the presence of long worms. Consequently, the sample does not flow even when the vial is tilted (top) and retains bubbles for a long time (bottom). Moreover, the sample shows flow-birefringence; i.e., when viewed under crossed polarizers, streaks of light appear when the sample vial is lightly shaken (bottom). (B) Upon UV irradiation, OMCA is isomerized to its *cis* form, leading to much shorter micelles. In turn, the sample viscosity is significantly reduced, as shown by its rapid pourability (top) and by the rapid rise of bubbles to the liquid surface (bottom). Also, the flow-birefringence is no longer observed (bottom).

Based on the different rheological responses induced by the *trans* and *cis* forms of OMCA in CTAB mixtures, we were interested in examining the effects of light irradiation on sample rheology. Accordingly, we irradiated the 60 mM CTAB + 50mM

OMCA sample with UV light for 30 min. Figure 3.3B presents visual evidence for the effects induced by UV irradiation on the sample rheology. The photographs show that the sample has been converted to a thin, runny fluid that can be easily poured out of the vial and in which bubbles rapidly rise to the surface. Moreover, the irradiated sample does not show flow-birefringence. Thus, Figure 3.3 demonstrates a dramatic light-induced rheological transition in the CTAB/OMCA sample. Based on the spectra in Figure 3.2, the rheological change is clearly a result of the *trans* to *cis* photoisomerization of OMCA. We will show that this change in molecular geometry causes a dramatic reduction in micellar length, which explains the drop in viscosity.

We now present rheological data on selected CTAB/OMCA samples to quantify the light-induced rheological changes. Note that, following irradiation, CTAB/OMCA samples remain unaltered when stored under ambient conditions (exposure to visible light has no effect because OMCA has a negligible absorbance in the visible range of the spectrum). Thus, irradiated samples could be tested subsequently on the rheometer. Figure 3.4 shows steady-shear rheological data (viscosity vs shear rate) for three samples, each containing 60 mM CTAB, with OMCA concentrations of 30, 50, and 80 mM, respectively. Before irradiation (Figure 3.4a), all three samples show shear-thinning behavior, with a plateau in the viscosity at low shear rates, followed by a decrease in viscosity at higher shear rates. The zero-shear viscosity η_0 is highest for the 50 mM OMCA sample, with a value of about 10 Pa·s (i.e., about 10,000 times the viscosity of water). With further increases in OMCA content, there is a drop in η_0 (this is further discussed under Figure 3.7), and the 80 mM OMCA sample has an η_0 value of about

2 Pa·s. Figure 3.4b shows the rheology of the same three samples after UV irradiation for 30 min. The irradiated samples show negligible dependence of their viscosities on shear rate; i.e., their behavior is mostly Newtonian (only the 80 mM OMCA sample shows a slight shear-thinning). Moreover, the viscosities are much lower compared to Figure 3.4a, with each sample showing a drop in η_0 by several orders of magnitude due to UV irradiation. The rheological measurements thus confirm the visual observations reported in Figure 3.3.

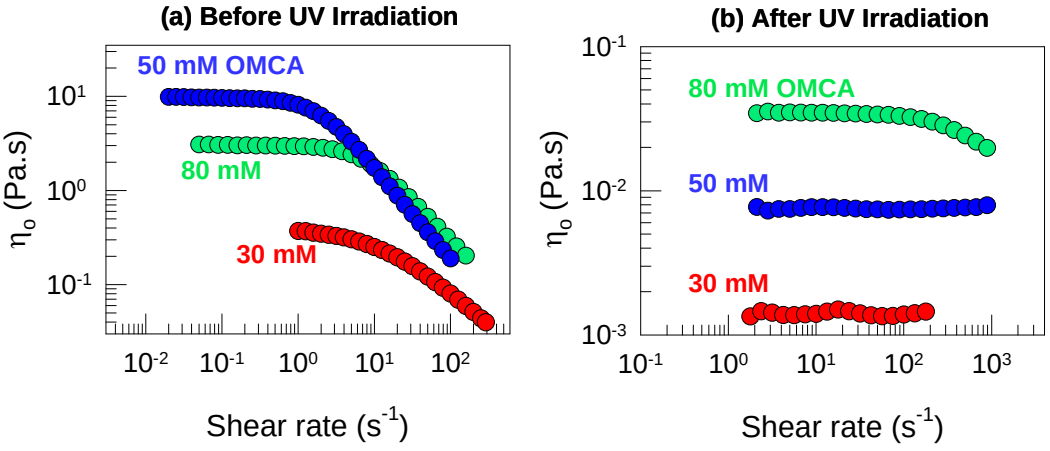

Figure 3.4. Viscosity vs. shear rate plots for three CTAB/OMCA mixtures (a) before and (b) after UV irradiation for 30 min. The samples each contain 60 mM CTAB, and their OMCA concentrations are indicated on the plots. All samples show a shear-thinning response before irradiation, whereas after irradiation, the samples are mostly Newtonian with much lower viscosities.

In addition to steady-shear rheology, it is useful to examine the rheological response under dynamic or oscillatory shear, which is a more sensitive probe of the structure in complex fluids (Section 2.4). Figure 3.5 shows dynamic rheological data on a sample containing 60 mM CTAB and 50 mM OMCA. The data are presented as plots of the elastic modulus G' and viscous modulus G'' as functions of the angular frequency ω.

Before irradiation (Figure 3.5a), the sample shows a typical viscoelastic response; i.e., the behavior is elastic ($G' > G''$, plateau in G') at high frequencies or short time scales, while it is viscous ($G'' > G'$, both moduli are strong functions of frequency) at low frequencies or long time scales. On the other hand, after irradiation with UV light for 30 min (Figure 3.5b), the sample exhibits a purely viscous response over the entire range of frequencies. Thus, dynamic rheology confirms a light-induced transition from a viscoelastic fluid to a thin, viscous one, again consistent with the photographs in Figure 3.3.

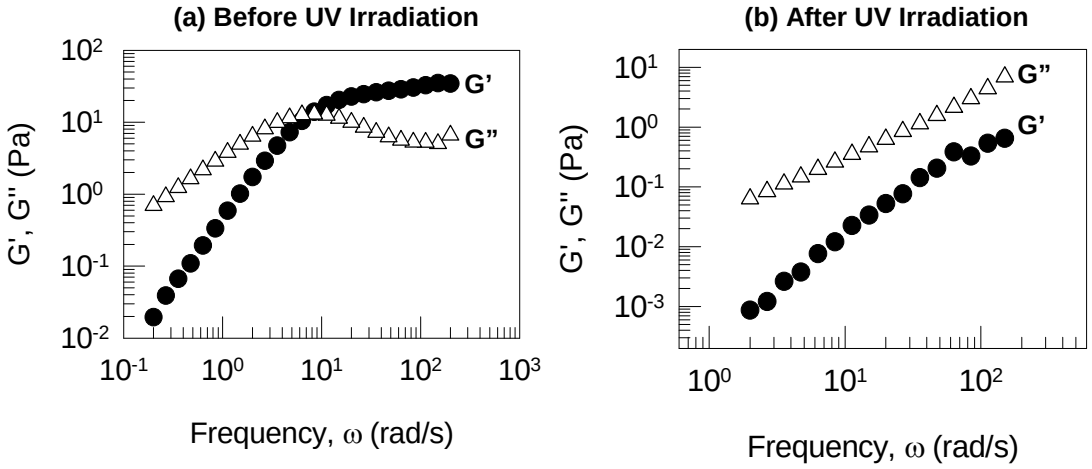

Figure 3.5. Dynamic rheology of a 60 mM CTAB + 50 mM OMCA sample (a) before and (b) after UV irradiation for 30 min. Before irradiation, the sample shows a viscoelastic response, whereas, after irradiation, its response is predominantly viscous.

We have thus shown that appreciable rheological changes can be induced in CTAB/OMCA samples by UV irradiation. Next, we discuss the evolution of sample rheology as a function of irradiation time. Figure 3.6 shows viscosity vs. shear rate plots for a 60 mM CTAB + 50 mM OMCA sample after various periods of UV irradiation. Before irradiation, the sample is highly viscous and strongly shear-thinning. After 10 min of irradiation, the zero-shear viscosity is reduced by about 2 orders of magnitude and the

extent of shear-thinning is also reduced. After 20 min, the viscosity is further reduced and the sample behaves like a Newtonian fluid over the shear rates investigated. Finally, after 37 min, the viscosity drops to that of the solvent, i.e., water. No further changes in viscosity occur with longer irradiation. The data shows that the viscosity drop can be controlled through the irradiation time. It is worth pointing out here that the rate of viscosity reduction is determined primarily by the rate of absorption of UV light by the sample, which in turn depends on the intensity of the UV lamp, the sample volume used, and the experimental geometry (path length). Once the OMCA molecules absorb light, they will photoisomerize rapidly (~ milliseconds). In the above experiments, we did not attempt to optimize the transition speed, but it is easy to achieve faster viscosity transitions with smaller sample volumes. Preliminary experiments with < 1 mL samples show that a significant viscosity drop can be achieved within a few seconds.

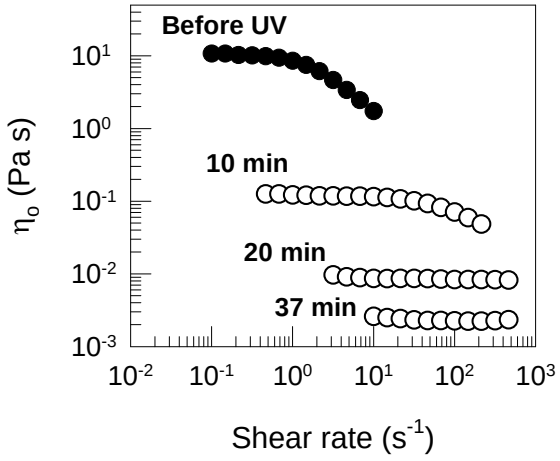

Figure 3.6. Steady-shear rheology of a 60 mM CTAB + 50 mM OMCA sample before irradiation and after UV irradiation for various periods of time (as indicated on the plot). The sample is observed to switch from a highly viscous, shear-thinning fluid to a low-viscosity, Newtonian fluid with progressive irradiation.

The viscosity drop upon UV irradiation can also be controlled via the sample composition itself. Figure 3.7 shows the zero-shear viscosity η_0 of 60 mM CTAB solutions as a function of either *trans*-OMCA or *cis*-OMCA concentration. For the *trans*-OMCA samples, data are also shown after 30 min of UV irradiation. Note that the viscosities of CTAB/*cis*-OMCA solutions are very low and approximately identical to that of water. On the other hand, the viscosities induced by *trans*-OMCA are much higher and reach a peak around 50 mM of the additive. Such a viscosity peak vs. additive concentration is often seen for wormlike micelles[39,40] and is believed to signify a transition from linear to branched worms. Upon UV irradiation of the *trans*-OMCA samples, the viscosities drop in all cases, with the extent of the drop being highest (ca. 10,000-fold) near the peak. It should be noted that, for all samples, irradiation for longer times would cause the viscosity to drop further until the photoisomerization is complete. Then, the viscosity will drop to that of the *cis*-OMCA samples, i.e., to a water-like value.

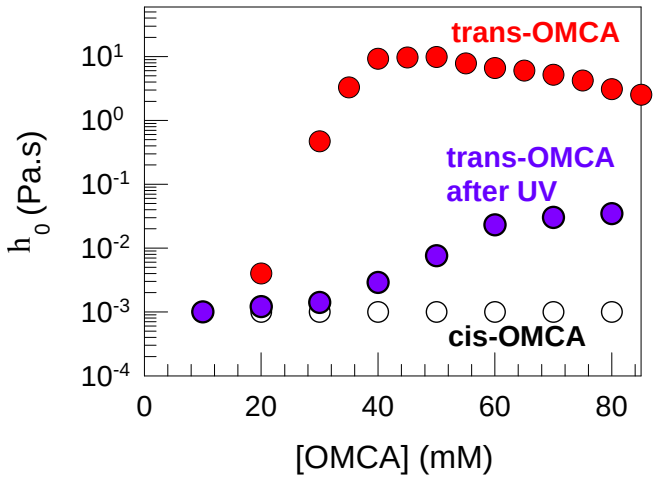

Figure 3.7. Zero-shear viscosity η_0 of 60 mM CTAB + OMCA mixtures as a function of the OMCA content. Data are shown for samples containing *trans*-OMCA, for *cis*-OMCA, and for *trans*-OMCA samples after 30 min of UV irradiation. A significant light-induced drop in viscosity is observed for the *trans*-OMCA samples.

The above rheological and visual observations on CTAB/OMCA samples indicate a transition from long, wormlike micelles to much shorter micelles upon UV irradiation. To recap, before irradiation, the samples are flow-birefringent, they are viscoelastic under dynamic rheology, and shear-thinning in steady rheology. All these phenomena are associated with wormlike micelles: the flow birefringence arises because the worms tend to align along the flow direction when sheared, the viscoelastic behavior is due to the entanglement of the worms into a transient network, and the shear-thinning is caused by a disruption of this network due to shear (see Section 2.2 also).[40,46] The absence of these phenomena in the irradiated sample suggests that the micelles have been reduced to much shorter (non-entangled) structures. In order to independently verify such a reduction in micellar size, we turn to a second technique, namely SANS.

Samples for SANS were made in D_2O to achieve the required contrast between the micellar structures and solvent. We verified that CTAB/OMCA samples in D_2O were rheologically identical to those made in H_2O. SANS data can be readily interpreted in terms of micelle size and shape only when intermicellar interactions (structure factor contributions) are minimized, i.e., when electrostatic interactions are screened and the micelle volume fraction is low. We therefore studied equimolar CTAB/OMCA samples at relatively low concentrations. SANS spectra (I vs q) are shown in Figure 3.8 for three samples with CTAB/OMCA concentrations of 30/30, 20/20, and 5/5 mM, respectively. In each case, data are shown before and after UV irradiation for 30 min. For all samples, irradiation is observed to cause a significant drop in the scattered intensity at low q. Such a drop in intensity is a direct, qualitative indication of a decrease in micelle size.

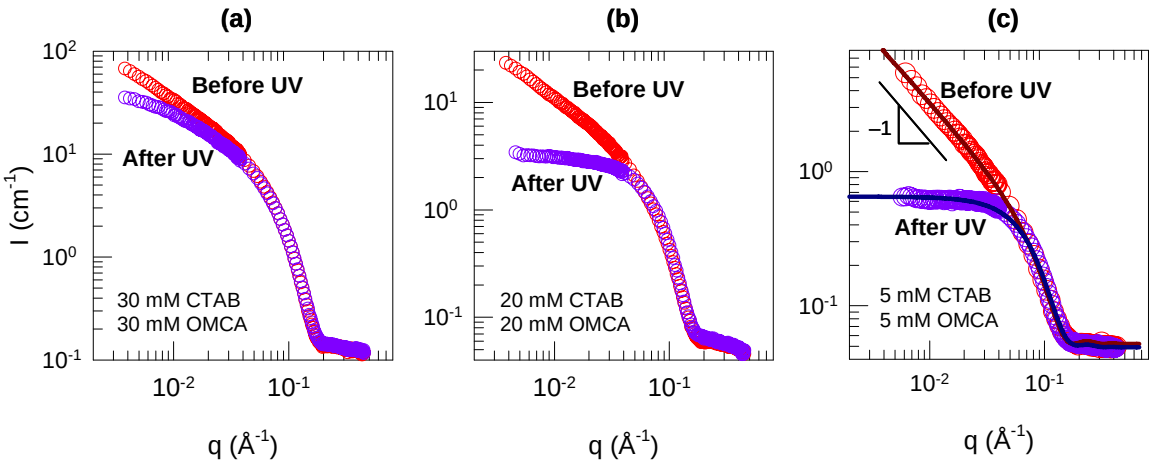

Figure 3.8. SANS scattering spectra from three CTAB/OMCA mixtures before and after 30 min of UV irradiation. The lines through the data for the 5/5 CTAB/OMCA sample are model fits to long, cylindrical micelles (before irradiation) and short, ellipsoidal micelles (after irradiation).

To obtain a more quantitative measure of micellar sizes, we model the SANS data from the 5/5 sample. For this sample (Figure 3.8c), a large decrease in intensity is seen upon UV irradiation, presumably because the micelle sizes fall within the window probed by SANS. Prior to irradiation, the intensity asymptotes at low q to a slope of about –1, which is indicative of long, cylindrical structures.[37] We therefore model the micelles as rigid cylinders (eqs 2.6, 2.7), and the fit is shown as a solid line through the data. From the fit, the micellar radius is obtained to be about 22 Å, while their length is ca. 3000 Å. The same sample after irradiation shows a plateau in SANS intensity at low q, which suggests the presence of smaller and more globular structures. Accordingly, we model the micelles in this case as ellipsoids of revolution (eq 2.5), and the corresponding fit is again shown as a solid curve through the data. A good fit is obtained for prolate ellipsoids with radii of 22 and 40 Å, respectively, for their major and minor axes. Thus, as expected,

there is a dramatic reduction in the largest dimension of the micelles (a factor of about 100) due to UV irradiation.

The SANS data thus confirm that the light-induced viscosity reduction in CTAB/OMCA mixtures is due to a decrease in micelle size. The micellar size reduction, in turn, is evidently caused by the photoisomerization of OMCA from *trans* to *cis*, as indicated by the UV-Vis spectra (Figure 3.2). Incidentally, some studies have shown that cinnamic acid can also undergo photodimerization.[45,47] To rule out this possibility in the case of OMCA, we used HPLC to study samples of CTAB/*trans*-OMCA and CTAB/*cis*-OMCA prior to UV irradiation, as well as CTAB/*trans*-OMCA following UV irradiation. Using HPLC, it is possible to quantify the presence of photodimers as well as their amounts relative to photoisomers.[45,47] Typical HPLC chromatograms for the three samples are shown in Figure 3.9. The irradiated CTAB/*trans*-OMCA sample (bottom plot) only shows three peaks, which correspond to NaOH, *cis*-OMCA, and *trans*-OMCA respectively, in order of increasing elution times. This sample was run in the HPLC column for 2 hours and no other peaks emerged at elution times beyond 15 min. If photodimers were present, they would have eluted from the column within a few minutes after the *trans*-OMCA.[45,47] Note also that the height of the *cis* peak is much greater than the *trans* peak, thereby showing that a *trans* to *cis* isomerization has indeed occurred upon irradiation. Thus, HPLC confirms that photoisomerization of OMCA is the dominant effect and that photodimerization is negligible. This finding is consistent with the results of Figure 3.7, which show that *trans* and *cis*-OMCA differ greatly in their ability to induce growth of CTAB micelles.

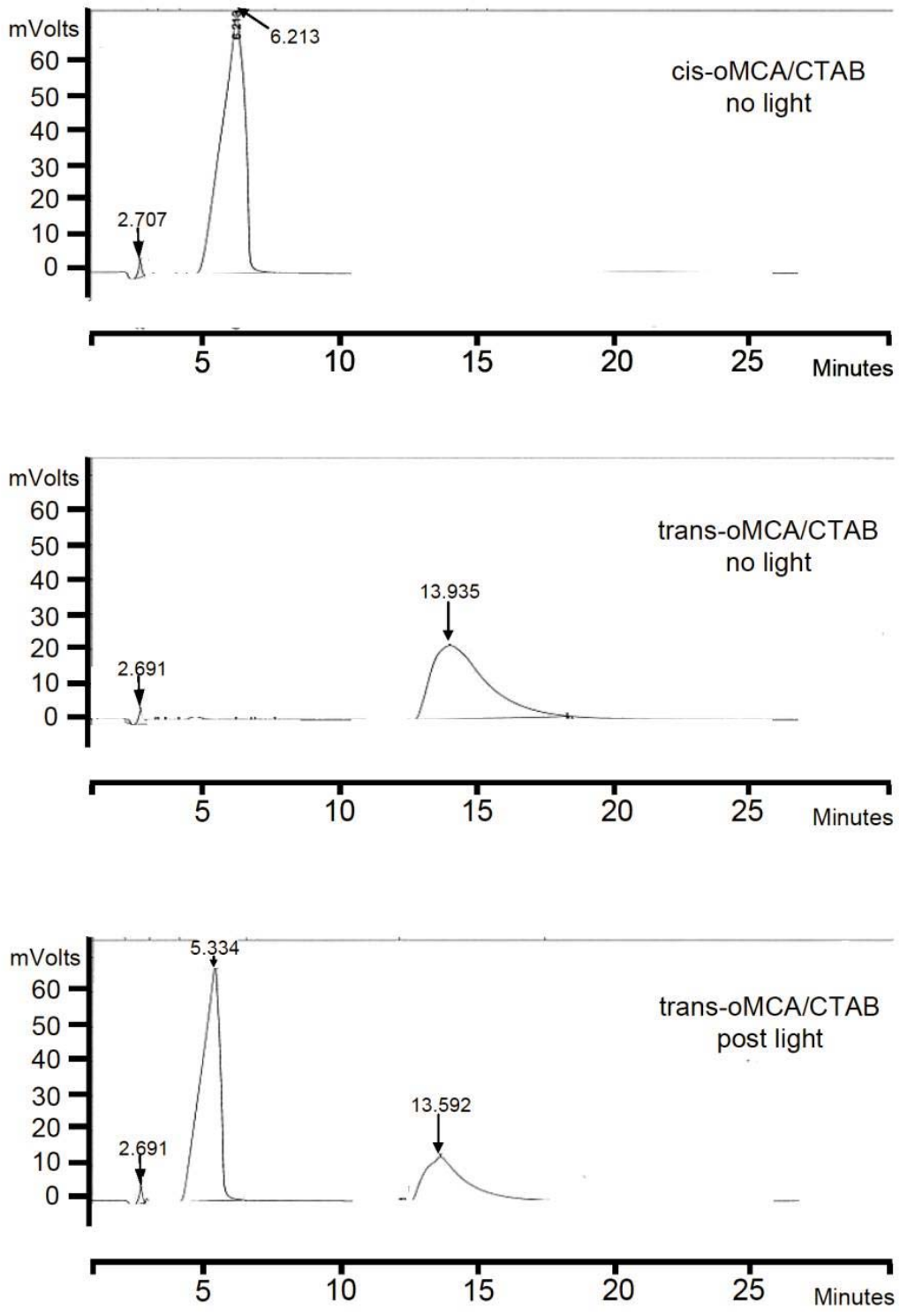

Figure 3.9. HPLC chromatograms for CTAB/*cis*-OMCA (top), CTAB/*trans*-OMCA before UV irradiation (middle), and CTAB/*trans*-OMCA after UV irradiation (bottom).

The question then is *why* are *trans*- and *cis*-OMCA so different in their effects on CTAB micelles? Can we rationalize these differences based on our knowledge of wormlike micelles and their self-assembly? We believe that there are two related factors to consider: (i) **the geometry** of the OMCA isomers, and (ii) **their hydrophobicities**. Both these factors will influence the binding of OMCA with CTAB micelles. As discussed in Section 2.2, the binding of aromatic counterions like OMCA will reduce the micellar surface charge and thus facilitate the growth of long wormlike micelles. In other words, the key requirement for micellar growth is the binding (adsorption) of OMCA counterions at the micellar interface.[40] OMCA is expected to adsorb in such a way that the phenyl ring is embedded in the hydrophobic interior of the micelle while the carboxylate anion is located next to the cationic headgroups at the surface.[46,48] Also, the extra methyl group on OMCA must be preferably oriented toward the micelle interior as well. Such an orientation is possible for *trans*-OMCA but more difficult for *cis*-OMCA (Figure 3.1). In the case of *cis*-OMCA, the methyl and carboxylate moieties are so close that it will be difficult for the former to orient inward and the latter outward relative to the micellar interface. In short, geometric arguments suggest that *trans*-OMCA can strongly associate with CTAB micelles, whereas *cis*-OMCA will associate weakly.

A second related argument concerns the relative hydrophobicities of the two isomers: specifically, we believe that *trans*-OMCA is more hydrophobic than *cis*-OMCA. A greater hydrophobicity of the *trans* isomer has been noted for a variety of compounds, including olefinic and azobenzene derivatives. For example, in azobenzene-based surfactants, the greater hydrophobicity of the *trans* form gives it a lower critical micelle

concentration (CMC).[8,9] This difference in hydrophobicity has been attributed to the lower net dipole moment of the *trans* compared to the *cis* isomer: i.e., the dipoles add up in the *cis*, while they tend to cancel each other in the *trans* (equivalently, there is greater charge delocalization in the *cis* form).[8,9] Moreover, our own studies further confirm the differences in hydrophobicity. In the absence of base, we find that *trans*- and *cis*-OMCA have limited solubility in deionized water. But while the solubility of *cis*-OMCA is measured to be 8.6 mM, the solubility of *trans*-OMCA is just 0.26 mM, i.e., more than a factor of 30 less. Accordingly, our solubility measurements confirm that *trans*-OMCA is much more hydrophobic than *cis*-OMCA, which suggests that the former will associate with the micelles to a much greater extent. Indeed, a lower solubility in water has been correlated with a greater association with micelles previously.[46] All in all, the hydrophobicity arguments support the geometric reasoning advanced above.

Our arguments ultimately lead to the following mechanism to explain our results: when *trans*-OMCA is mixed with CTAB, the counterions will strongly bind to CTAB micelles, causing growth of worms. Upon UV irradiation, *trans*-OMCA is converted to *cis*-OMCA, which has a much weaker interaction with CTAB, and will therefore tend to desorb from the micellar interface. As a result, the effective area of CTAB headgroups will increase, causing the worms to transform into much smaller structures and, thereby, driving the sharp drop in solution viscosity.

Last, it is worth discussing the generality of our results as well as the reversibility of the viscosity changes. We have observed similar light-induced viscosity transitions

with several aromatic derivatives similar to OMCA, including cinnamic acid and *ortho*-coumaric acid. Thus, the results and mechanism presented here should extend to a range of aromatic derivatives. With regard to reversing the viscosity changes, we note from the UV-Vis spectra that *trans*-OMCA has a much higher absorption than *cis*-OMCA over the entire wavelength range, which precludes a reverse *cis* to *trans* photoisomerization (but an acid-catalyzed reversal by heat is possible[49]). Nevertheless, a variety of other organic molecules do permit reversible photoisomerizations,[42] and the key will be to employ a molecule whose photoisomers have different effects on micellar self-assembly. This is further discussed in the following chapters.

3.4 Conclusions

We have demonstrated light-tunable rheological properties in a class of micellar fluids consisting of the cationic surfactant, CTAB, and the organic derivative, OMCA. When OMCA is in its *trans* form, it binds strongly with CTAB, leading to the formation of wormlike micelles. These micelles entangle into a transient network and thereby give rise to a highly viscoelastic fluid. Upon irradiation by UV light, *trans*-OMCA is isomerized to *cis*-OMCA. The *cis* isomer has a much weaker interaction with CTAB since its geometry does not favor binding at the micellar interface and because it is more hydrophilic. Consequently, the *cis* isomer tends to desorb from the micellar interface, transforming the micelles into smaller structures, and the sample thus becomes a low-viscosity, Newtonian fluid. A drop in zero-shear viscosity by several orders of magnitude can be induced in these fluids upon light irradiation for a few minutes. Such fluids could thus be promising for use in microscale flow-control devices and sensors.

Chapter 4

Non-Aqueous Photogelling/Photothinning Fluids

4.1 Introduction

In this chapter, we are interested in extending the PR concept to non-polar organic solvents. Previous work on light-induced viscosity changes have included some studies on non-aqueous systems. Again, the photoresponsive molecules in these earlier studies were invariably created by specialized chemical synthesis. For example, Eastoe et al.[50] synthesized a stilbene containing photo-surfactant and used it to develop a photoresponsive organogel in toluene. Similarly, Shinkai and co-workers[44] synthesized an azobenzene-modified cholesterol and created photoresponsive organogels with this molecule in a range of organic solvents. The latter gel was a photoreversible system: upon irradiation with UV light, the gel was disrupted into a sol while subsequent irradiation of the sol with visible light caused the gel to reform. As stated previously, the need for complicated synthesis schemes to prepare such novel molecules limits the availability of the above systems for both research and commercial use.

Our goal, then, is to design PR fluids based on organic solvents in much the same way as we did in Chapter 3 – i.e., with simple, inexpensive molecules that can be purchased from commercial vendors. A starting point for our study is the behavior of amphiphilic molecules (lipids and surfactants) in organic solvents – an area in which our

laboratory has accumulated extensive experience. It is well-known[25,51-55] that certain amphiphiles can form "reverse" wormlike micelles in organic solvents. As discussed in Section 2.4, the most widely used recipe for forming such reverse worms is by adding a small amount of water to an organic solution of the phospholipid, lecithin. Like normal worms, these reverse worms are also long, flexible cylindrical chains, but with their molecular structure inverted, i.e., with the nonpolar surfactant tails on the outside and the polar surfactant heads on the inside of the cylinder.

Now let us consider the typical recipe for reverse worms and see how we can impart photoresponsive properties to such a system. A commonly used solvent is cyclohexane and we can therefore consider mixtures of lecithin/water/cyclohexane. The literature on reverse worms surprisingly has little discussion on how additives to the above system might influence its rheology. When considering additives, one needs to take into account their polarity. For example, highly non-polar additives would simply dissolve in the solvent (cyclohexane) and therefore might have little effect on the micellar structure. On the other hand, highly polar additives (e.g., salts) might be completely insoluble in these organic fluids. The key therefore is to find an additive that is photoresponsive while at the same time at least weakly soluble in the presence of the reverse micelles. If such an additive could be found, it is still difficult to predict *a priori* how (or how much) the additive would influence the fluid rheology in either its ground state or upon irradiation.

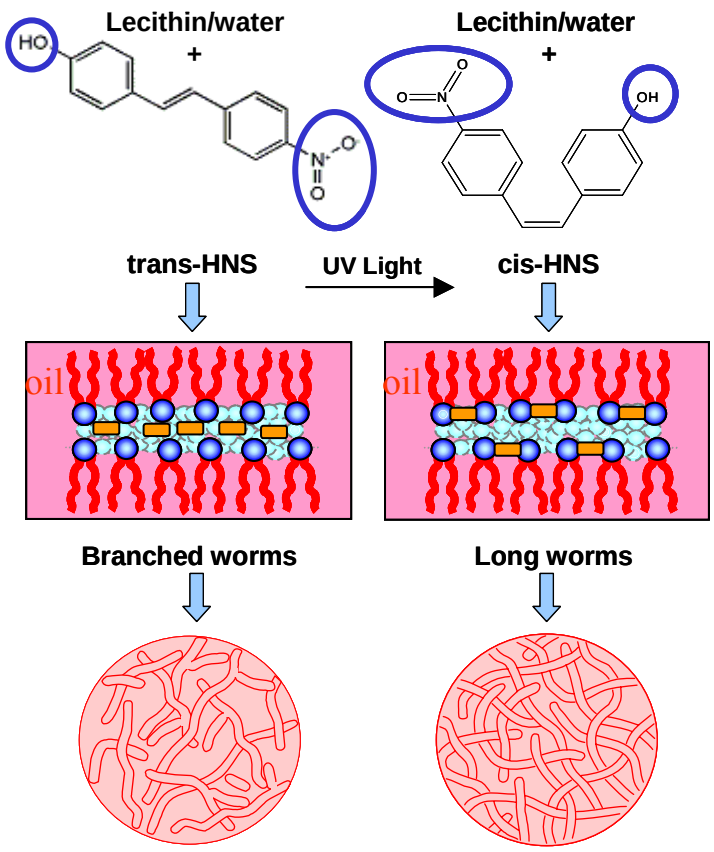

Figure 4.1. Schematic behavior of non-aqueous PR fluids consisting of lecithin, HNS and water in cyclohexane. When HNS molecules are in their *trans* form, the molecules are believed to reside in the interior of the reverse micelles. Upon UV irradiation, *trans*-HNS gets photoisomerized to *cis*-HNS and the *cis* isomers are postulated to move to the micellar interface. These molecular changes are, in turn, believed to cause a transition from branched to linear reverse cylindrical micelles, resulting in an increase in zero-shear viscosity (photogelling).

Based on the above discussion, the task of designing a non-aqueous PR fluid based on reverse micelles appears to be quite a daunting one. Nevertheless, we have indeed been able to develop a fluid formulation that displays significant light-sensitivity in its rheological properties. The key molecule in our formulation is the stilbene derivative, 4-hydroxy-4'-nitrostilbene (HNS), which is capable of undergoing a *trans* to *cis* photoisomerization about its double bond under UV light (Figure 4.1) (see also Section 2.5). We add HNS to the "traditional" lecithin/water/cyclohexane mixtures to

obtain a class of non-aqueous PR fluids. Certain compositions of the above mixtures undergo photogelling: i.e., the zero-shear viscosities of these fluids increase by as much as *four orders of magnitude* upon UV irradiation. Interestingly, other compositions show the opposite behavior, i.e., their viscosities decrease upon UV irradiation. Thus, the composition dictates the direction and magnitude of light-induced rheological changes. From a microstructural standpoint, the interpretation of these results is not quite as straightforward as that for the aqueous PR fluids in Chapter 3. However, we offer below a plausible hypothesis to explain our key results. The main concept, as suggested by Figure 4.1, is that one of the isomers of HNS is more interfacially active than the other.

4.2 Experimental Section

Materials. Lecithin (> 98% purity) from Avanti Polar Lipids, *trans*-HNS (> 98%) from Alpha Aesar, and cyclohexane from Sigma were purchased and used as received. Ultrapure deionized water from a Millipore water purification system was used in preparing samples. The samples were prepared by dissolving weighed amounts of lecithin and HNS in cyclohexane and then adding water using a micropipette to reach the final composition. Samples were stirred continuously for 2 days and then left to equilibrate overnight in a desiccator at room temperature before any experiments were conducted.

Sample Response Before and After UV Irradiation. Samples were irradiated with UV light from an Oriel 200 W mercury arc lamp. To access the desired wavelength of emitted light, a dichroic beam turner with a mirror reflectance range of 350 to 450 nm was used along with a < 400 nm filter. Samples (5 mL) were placed in a Petri dish with a quartz

cover and were irradiated for a specific duration under stirring. Due to the nature of the HNS spectra, irradiated samples did not undergo any changes when stored in the dark under ambient conditions (to be additionally careful, we generally covered sample vials with aluminium foil), which made it easy to conduct subsequent tests. UV-Vis spectroscopy before and after irradiation was carried out using a Varian Cary 50 spectrophotometer.

Rheological Studies. Steady and dynamic rheological experiments were performed on an AR2000 stress controlled rheometer (TA Instruments, Newark, DE). Samples were run at 25°C on a cone-and plate geometry (40-mm diameter, 2° cone angle) or a couette geometry (rotor of radius 14 mm and height 42 mm, and cup of radius 15 mm). Dynamic frequency spectra were obtained in the linear viscoelastic regime of each sample as determined by dynamic stress-sweep experiments.

4.3 Results and Discussion

We first describe the effect of *trans*-HNS on lecithin/water/cyclohexane reverse micelles at a fixed lecithin concentration of 100 mM. Figure 4.2 presents the zero-shear viscosity η_0 of such solutions as a function of water content. The values of η_0 were obtained from steady-shear rheological experiments in the limit of low shear rates, where the viscosity asymptotically approached a plateau. The x-axis on the plot is the water:lecithin molar ratio w_0. For solutions containing no *trans*-HNS (open circles), there is a peak in η_0 at a w_0 of about 8 and the viscosity drops with further addition of water. Such a viscosity peak has been observed before for lecithin/water/cyclohexane reverse

worms and similar peaks are observed for reverse worms in other solvents as well.[56-60] Although the precise significance of the viscosisty maximum is still not known, it is believed to signify a transition from linear to branched worms.[56-60] Now let us examine the effect of adding *trans*-HNS to the above system. *trans*-HNS is, in fact, insoluble in neat cyclohexane but it can be dissolved in small amounts in the presence of lecithin micelles. We add 15 mM of *trans*-HNS to each of the lecithin/water/cyclohexane samples and again measure their zero-shear viscosities. The new η_0 data (red circles) again show a peak as a function of w_0, but the peak is shifted to higher values of w_0 (about 12). Moreover, the entire curve is shifted to significantly lower η_0 values – i.e., *trans*-HNS lowers the viscosity by orders of magnitude regardless of the water content in the sample.

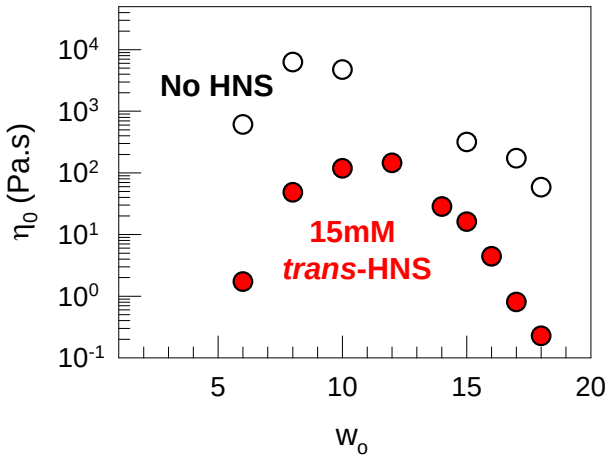

Figure 4.2. Zero-shear viscosity η_0 of 100 mM lecithin/15 mM HNS mixtures as a function of the water:lecithin molar ratio w_0. For comparison, data are also shown for samples containing no HNS. A significant drop in viscosity is observed at upon addition of *trans*-HNS regardless of the water content in the sample.

We now present UV-Vis spectra for *trans*-HNS before and after irradiation (Figure 4.3). These experiments were done on samples of 0.75 mM *trans*-HNS in

cyclohexane in the presence of lecithin and water. The *trans*-HNS shows an absorbance peak in the UV range of the spectrum at 383 nm. When the above solution is irradiated with 350-400 nm UV light, *trans*-HNS undergoes an UV-induced photoisomerization to *cis*-HNS, as expected. This is reflected in the UV-Vis spectrum after irradiation, which shows a new peak at shorter wavelengths (263 nm) while the peak at 383 nm drops in intensity. In principle, the slightly higher absorbance of *cis*-HNS around 260 nm compared to its *trans* isomer implies that irradiation at this wavelength could possibly reverse the isomerization. However, this is difficult to achieve in practice because the absorbances are too close for the two isomers.

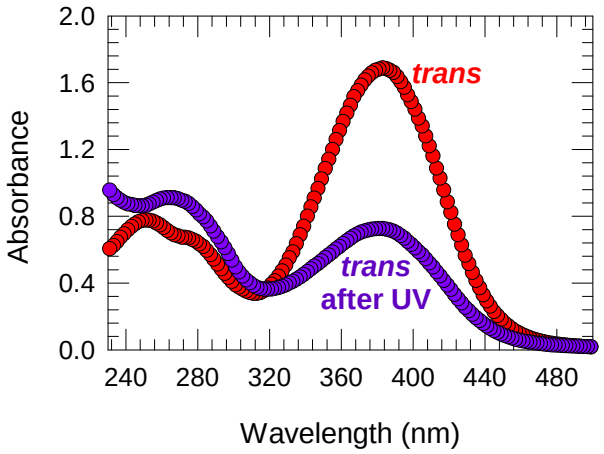

Figure 4.3. UV-Vis spectra of *trans*-HNS before and after after UV irradiation. The drop in absorbance at the higher wavelengths and increase in absorbance at the lower wavelengths after UV irradiation indicates that the molecule has been photoisomerized from *trans* to *cis*.

Having established that HNS can be photoisomerized, we consider the effect of this photoisomerization on the rheological properties of lecithin/HNS/water mixtures in cyclohexane. Henceforth, the abbreviation HNS will be used to refer to its *trans* form, which is the common, commercially available isomer (on the other hand, *cis*-HNS will be specifically denoted as such). Figure 4.4 presents the same zero-shear viscosity data as a function of water content for 100 mM lecithin/15 mM HNS samples as was shown in Figure 4.1; now, data are additionally shown for each of these samples after irradiation with UV light for 2 h. The data show an interesting trend: for w_0 values below the viscosity peak, we find that UV irradiation causes a drop in η_0. On the other hand, at higher water contents, specifically for w_0 beyond the peak (> 12), UV irradiation significantly increases the viscosity. The data thus show that the direction (increase or decrease) as well as the magnitude of light-induced rheological changes depends on the sample composition, in particular its location relative to the original viscosity peak.

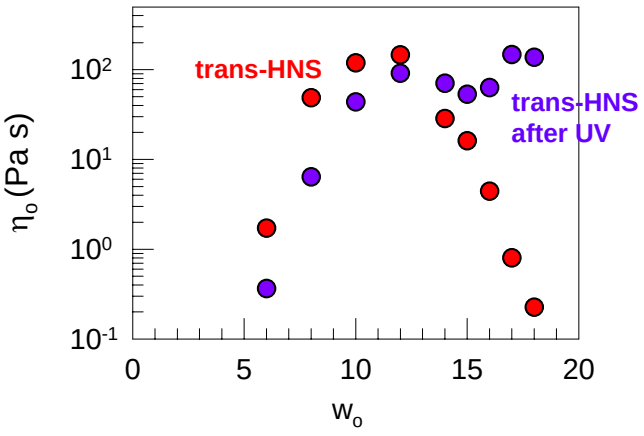

Figure 4.4. Zero-shear viscosity η_0 of 100 mM lecithin/15 mM HNS mixtures as a function of the water:lecithin molar ratio w_0. Data are shown before and after UV irradiation. A significant light-induced increase in viscosity is observed for samples at high w_0, while samples at low w_0 show a drop in viscosity.

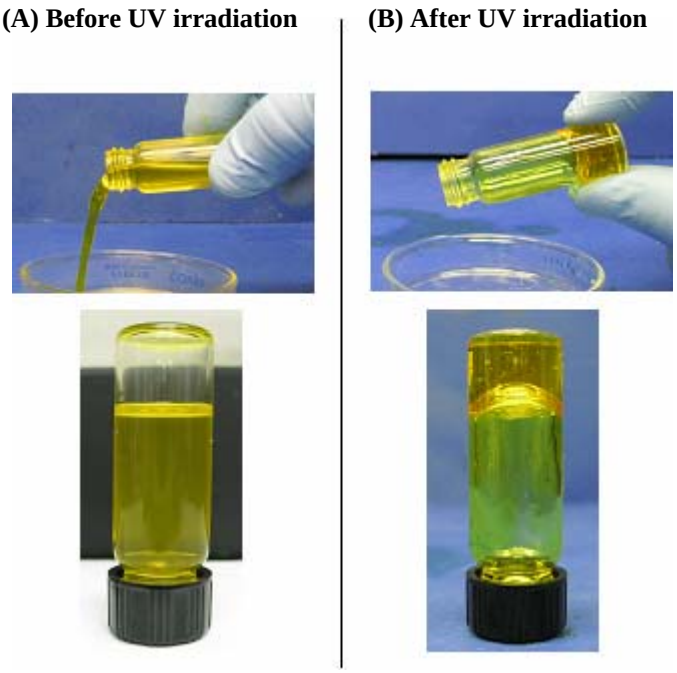

Figure 4.5. Photographs of a 100 mM lecithin/15 mM HNS/water (w_0 = 18) sample in cyclohexane (A) before and (B) after UV irradiation. (A) Initially, HNS is in its *trans* form and the sample has a low viscosity. Consequently, the sample flows rapidly out of a tilted vial (top) and to the bottom of the inverted vial (bottom). (B) Upon UV irradiation, HNS is isomerized to its *cis* form. In turn, the sample is photogelled: i.e., it becomes highly viscous and gel-like. Accordingly, the sample does not flow easily out of the tilted vial (top) and holds its weight in the inverted vial (bottom).

In Figure 4.4, the greatest increase in η_0 (c.a. 10,000 fold) occurs for the sample at w_0 = 18 and it is useful to study this sample further. Photographs of this sample before and after UV irradiation are shown in Figure 4.5. Before irradiation, the sample is a low-viscosity solution: it can be poured easily out of a tilted vial and bubbles rise to the liquid surface rapidly. Upon irradiation, the sample is converted into a viscoelastic, gel-like fluid. The sample does not readily flow out of a tilted vial – in fact, the bottom photograph shows that the sample can hold its weight in an inverted vial for short periods of time. Also, if bubbles are introduced into the sample by shaking the vial, they

remained trapped for extended periods of time. The sample also shows flow-birefringence, i.e., when the sample is viewed through cross polarizers, streaks of light appear upon shaking or tapping the vial (no such flow-birefringence is observed in the original sample before irradiation). Thus, Figure 4.5 demonstrates that light induces "photogelling", i.e., a substantial increase in viscosity and viscoelastic properties, for this lecithin/HNS/water solution in cyclohexane.

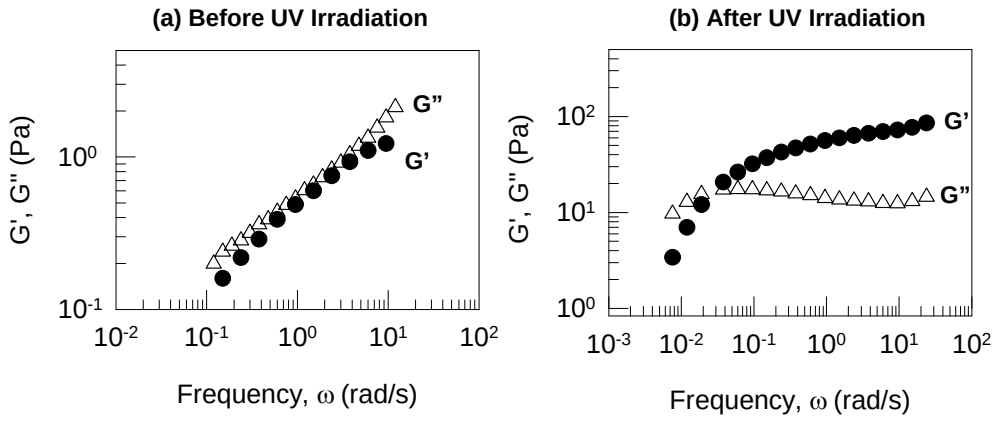

Figure 4.6. Dynamic rheology of a 100 mM lecithin/15 mM HNS/water (w_0 = 18) sample in cyclohexane (a) before and (b) after UV irradiation for 2 hr. Before irradiation, the sample shows a viscous response whereas after irradiation its response is viscoelastic.

The above visual observations for the w_0 = 18 sample can be further quantified through dynamic and steady-shear rheological experiments. First the dynamic rheological data are shown in Figure 4.6 before and after UV irradiation. These are plots of the elastic modulus G' and viscous modulus G'' as functions of the angular frequency ω. Before irradiation (Figure 4.6a), the sample shows a purely viscous response over the entire range of angular frequencies (since G'' is higher than G' and both moduli show a strong

dependence on frequency). After UV irradiation for 2 h (Figure 4.6b), the sample shows a typical viscoelastic response; i.e., at short time scales (high frequencies) the behavior is elastic ($G' > G''$, with G' asymptoting to a plateau), while at longer time scales (low frequencies), the response is viscous. The inverse of the frequency at which G' and G'' intersect gives a measure of the relaxation time of the sample, which is ca. 50 s in this case. The dynamic data are thus in accord with the visual observations of Figure 4.5 regarding the effect of UV irradiation on rheological properties.

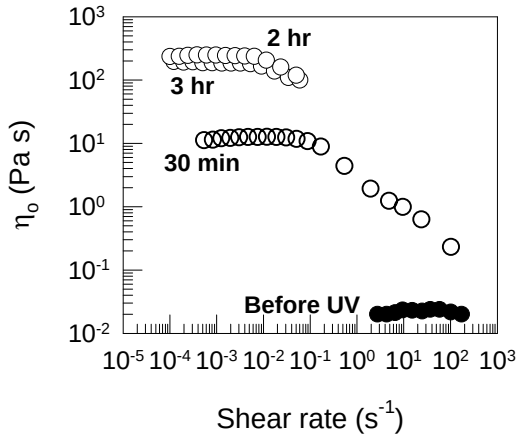

Figure 4.7. Steady-shear rheology of a 100 mM lecithin/15 mM HNS/water (w_0 = 18) sample in cyclohexane before irradiation and after UV irradiation for various periods of time (as indicated on the plot). The sample transforms from a low-viscosity Newtonian fluid, to a highly viscous shear-thinning fluid with progressive irradiation.

The corresponding steady-shear rheological data for the w_0 = 18 sample are plotted in Figure 4.7 with data being shown for different periods of UV irradiation. Before irradiation, the sample shows a low, constant viscosity (20 mPa·s) nearly independent of shear-rate, i.e., it shows Newtonian behavior. Upon irradiation, the sample becomes non-Newtonian and shear-thinning: the viscosity shows a plateau at low shear-rates followed by a drop at higher shear-rates. After 30 min of irradiation, the zero-

shear viscosity is increased by 3 orders of magnitude and subsequent irradiation to a total of 2 h increases η_0 by one further order of magnitude. Further irradiation beyond 2 h has negligible effect on the viscosity. As in Chapter 3, we should point out that the time required to alter the viscosity depends on sample volume, container size and path length. With smaller sample volumes, the time can be reduced considerably.

We would now like to discuss why we observe these light-induced changes in rheology, i.e., what are the mechanistic underpinnings of these effects? Upon UV irradiation, why does the viscosity go down if the composition lies to the left of the maximum (as a function of w_0) in Figure 4.3, and conversely, why does the viscosity go up to the right of the maximum? Given that a photoisomerization of HNS is taking place, why do the *trans* and *cis* forms of HNS have different effects on lecithin reverse micelles? As in Chapter 3, we believe the main factor to be the differences in geometry between the two HNS isomers. The *trans* form of the HNS molecule has polar end groups sticking out on *opposite* sides of the molecule (Figure 4.1), thus preventing it from having distinct hydrophilic and hydrophobic sides. In contrast, the *cis* form of the HNS molecule has the polar end groups on the same side of the molecule (Figure 4.1), leading to distinct hydrophilic and hydrophobic sides. We believe this makes the *cis*-HNS much more surface active than the *trans*-HNS.

The consequence of higher surface activity of the *cis* is as follows. Initially, when *trans*-HNS is mixed with lecithin/water in an organic solvent, the trans-HNS will not strongly bind at the interface and will instead reside in the core of the reverse micelles.

On the other hand, when *trans*-HNS is converted to *cis*-HNS, the cis isomer will move to the micellar interface orienting in such a way that its polar groups are directed inward and its nonpolar side faces outward. In effect, the HNS is replacing water molecules at the micellar interface and acting as glue between lecithin headgroups. *The result is to shift the viscosity curve in the direction of lower* w_0 *values*. For samples to the right of the viscosity maximum, a shift to lower w_0 implies an increase in the viscosity. On the other hand, for samples to the left of the maximum, a shift to lower w_0 would lower the viscosity. The above mechanism thus offers a tentative, but plausible, framework within which to interpret our results.

4.4 Conclusions

We have designed a class of non-aqueous photoresponsive fluids based on inexpensive, readily available molecules: namely, lecithin, water, and a photoresponsive stilbene, HNS. When HNS is in its *trans* form, it partitions to the interior of reverse micelles. Upon irradiation with UV light, *trans*-HNS isomerizes to *cis*-HNS. The *cis* isomer is interfacially active and the molecules thus shift their location to the micellar interface. In turn, the rheological properties of the fluid are affected, with the viscosity decreasing for certain compositions (low water content) and increasing at others (high water content). In particular, certain samples undergo photogelling, i.e., they are transformed from low-viscosity solutions to viscoelastic, gel-like fluids upon UV irradiation. The zero-shear viscosity can be increased by a factor of 10,000 in such cases. Our study thus offers a rational approach to exploiting molecular self-assembly in the design of light-responsive organic fluids.

Chapter 5

Photoreversible Aqueous Fluids

5.1 Introduction

The studies discussed in both Chapter 3 and 4 provided a drastic change in the viscosity, but we were not able to reverse the PR response. To create a system that has a reversible photorheological response, we developed an aqueous PR fluid using an azobenzene derivative as the additive. As mentioned in Section 2.3, azobenzene molecules tend to show a clean reversible photoisomerization. To our knowledge, only a few other groups have developed reversible PR fluids,[8-10,44] but these PR fluids require the complicated synthesis of azobenzene modified surfactants. In this chapter, we report a new class of reversible PR fluids that are based entirely on simple, inexpensive chemicals available to any laboratory. We have combined an azobenzene derivative, 4-azobenzene carboxylic acid (ACA), into micelles of the cationic surfactant erucyl bis(2-hydroxyethyl)methyl ammonium chloride (EHAC). In certain EHAC/ACA samples, we have found an increase in viscosity upon UV irradiation, which correlates with a *trans* to *cis* isomerization (much like for CTAB/OMCA and Lecithin/HNS systems) In addition, when the sample is exposed to subsequent visible light, we have observed a decrease in viscosity, which corresponds to a *cis* to *trans* reverse isomerization. The basis for this viscosity change is the *trans* to *cis* and *cis* to *trans* photoisomerization of the double bond in ACA (Figure 5.1). As in chapter 3, the resultant change in the geometry of ACA alters

the molecular packing of the EHAC/ACA complex, leading to an increase in the micellar length following UV irradiation and a subsequent decrease in the length with visible light irradiation (Figure 5.1). This change in viscosity can be repeated (thin-thick-thin-thick-etc), leading to a substantial reversible change in viscosity that can be cycled many times over.

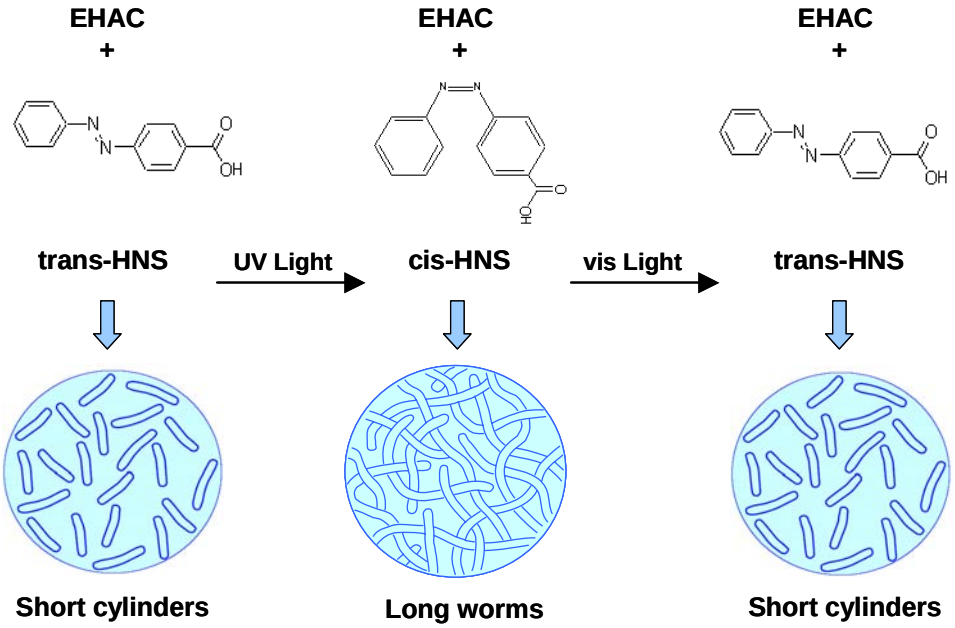

Figure 5.1. Schematic behavior of photoresponsive (PR) fluids consisting of EHAC and ACA. When ACA is in its *trans* from, its mixture with EHAC gives rise to short cylindrical micelles. Upon UV irradiation, *trans*-ACA photoisomerizes to *cis*-ACA, and the corresponding change in molecular geometry causes an increase in the length of the micelles. Upon subsequent irradiation with visible light, *cis*-ACA isomerizes back to *trans*-ACA, and the corresponding change in molecular geometry cause the system to revert back to the original short cylindrical micelles.

5.2 Experimental Section

Materials. EHAC was purchased from Akzo Nobel, Chicago, IL, and ACA in its *trans* form was purchased from TCI and was greater than 98% in purity. All chemicals were used as received. Ultrapure deionized water from a Millipore water purification system was used in preparing samples for visual observations and rheological characterization. Solutions were prepared by dissolving weighed amounts of dried EHAC in DI water followed by the addition of desired amounts of ACA with a slight excess of base (NaOH) to reach the final composition. Samples were stirred continuously under mild heat until they became homogeneous. The solutions were then left to equilibrate overnight at room temperature before any experiments were conducted. The pH in the samples was 7.

Sample Response Before and After UV Irradiation. EHAC/ACA samples were irradiated with UV light from an Oriel 200 W mercury arc lamp. A dichroic beam turner with a mirror reflectance range of 350 to 450 nm was used to access the desired UV range of the emitted light. We used a < 400nm filter to filter out the undesired visible wavelengths for the forward irradiation, and a > 400nm filter to filter out the undesired UV wavelengths for the reverse irradiation. Samples (2.5 mL) were placed in a Petri dish with a quartz cover, and irradiation was done for a specific duration under stirring. Due to the nature of the azobenzene molecules, discussed in Chapter 2, the molecule will revert back to its *trans* form under visible light and in the dark (slowly), this made it difficult to do subsequent tests with appropriate techniques. To keep the visible light from causing an undesired reverse transition, the samples were stored covered with aluminum foil. Also, all measurements were preformed directly after irradiation to overcome the slow reverse

transition in the dark. UV-Vis spectroscopy before and after irradiation was carried out using a Varian Cary 50 spectrophotometer.

Rheological Studies. Steady and dynamic rheological experiments were performed on an AR2000 stress controlled rheometer (TA Instruments, Newark, DE). Samples were run at 25°C on a cone-and-plate geometry (40-mm diameter, 2° cone angle) or a couette geometry (rotor of radius 14 mm and height 42 mm, and cup of radius 15 mm). Dynamic frequency spectra were obtained in the linear viscoelastic regime of each sample, as determined by dynamic stress-sweep experiments.

5.3 Results and Discussion

We first determine the effect ACA has on micellar mixtures of EHAC at a fixed EHAC concentration of 40 mM. Figure 5.2 presents the zero-shear viscosity, $\eta_{0,}$ of the EHAC/ACA solutions as a function of ACA concentration. The graph shows a peak in the zero-shear viscosity at an ACA concentration of about 10 mM, followed by a decrease in η_0 with increasing [ACA]. This peak in η_0 is often seen in wormlike micellar samples.[39,40] The shear-shear viscosity decreases to an order of magnitude greater than that of water at an ACA concentration of 22 mM. For the remainder of the study we focus on this low viscosity sample of 40 mM EHAC/ 22 mM ACA.

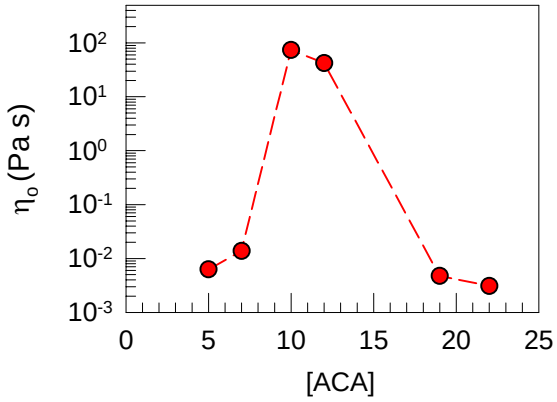

Figure 5.2. Zero-shear viscosity, η_0, of 40 mM EHAC + ACA mixtures as a function of ACA concentration.

Next we studied the effect of light on the molecular scale (photoresponsive molecule) of the system. To do this, we first present UV-Vis spectra for *trans*-ACA before irradiation, after UV irradiation, and after visible irradiation in Figure 5.3. These experiments were done with aqueous solutions containing 1 mM of ACA, 1.8 mM EHAC and 1 mM NaOH, with a baseline consisting of 1.8 mM EHAC and 1 mM NaOH. Figure 5.2 shows that the *trans* form has an absorbance peak at c.a. 320 nm. Thus, irradiation of the *trans* derivative with UV light will cause the molecule to absorb light, and this, in turn, can trigger a photoisomerization to its *cis* state. As discussed in Section 2.3, azobenzene molecules are expected to go through a clean reversible photoisomerization. To test whether this photoisomerization occurs for ACA, we irradiated the *trans*-ACA solution with UV light (350-400 nm) and recorded UV-Vis spectra after irradiation (Figure 5.1). The spectrum of ACA after UV irradiation shows a drop in the 320 nm peak and an increase in a peak at c.a. 440 nm, indicating a *trans* to *cis* isomerization. Based on the spectra, subsequent irradiation with visible light should cause the molecule to isomerize back to its *trans* form. Figure 5.3 also shows the spectra of the

ACA molecule after visible light irradiation. This spectrum shows a drop in the 440 nm peak and an increase in the 320 nm peak. Thus, the spectra shifted back to the original *trans*-ACA spectra, indicating the reverse *cis* to *trans* photoisomerization. Notice that while the reverse photoisomerization is possible, the UV-Vis spectra indicate the molecule does not reverse back 100% to its *trans* form.

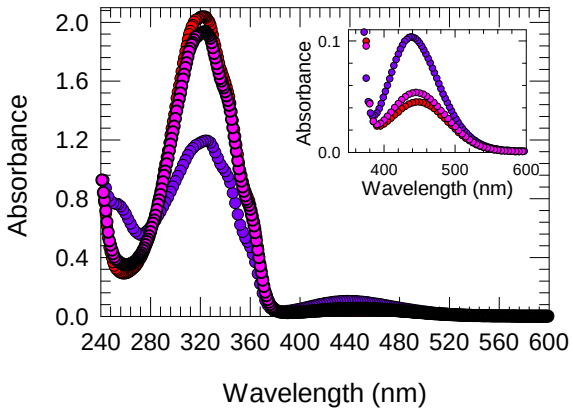

Figure 5.3. UV-Vis spectra of *trans*-ACA before irradiation, after UV irradiation, and after subsequent visible irradiation. The sample contains 1 mM of the HNS. The drop in absorbance at the UV wavelength and increase in absorbance at the visible wavelength in the *trans*-ACA curve after UV irradiation indicates that the molecule has been photoisomerized to its *cis* form. The subsequent increase in absorbance at the UV wavelength and decrease at the visible wavelength indicates the reverse *cis* to *trans* photoisomerization. The insert shows a blow up of the peaks in the visible wavelength range.

Next, we consider the macro-scale effect of light irradiation on our EHAC/ACA system. To do this we first mixed the photoresponsive molecule *trans*-ACA with EHAC, with a slight excess of base. Henceforth, the abbreviation ACA will be used to refer to its *trans* form, which is the common, commercially available isomer. (On the other hand, *cis*-ACA will be specifically denoted as such). From our initial studies we found that certain mixtures of EHAC and ACA could form low-viscosity, Newtonian solutions. For

example, Figure 5.4 shows photographs of a sample containing 40 mM EHAC and 22 mM ACA. This sample is water-like, such that it flows readily out of a tilted vial and bubbles rise readily to the surface (Figure 5.4A). Also, when the sample is stirred it does not stick to the stir bar (it does not show the rod climbing effect). We then irradiated the sample with UV (350-400nm) light. Figure 5.4B presents visual evidence of the properties of the sample after UV irradiation. The photographs show that the sample has become highly viscous and viscoelastic, the sample does not flow easily out of a tilted vial and when bubbles are introduced they do not easily rise to the surface. Also, when the sample is stirred it sticks to the stir bar, similar to the rod climbing effect. Taken together, the viscoelasticity and rod-climbing effect suggest the presence of long wormlike micelles (Section 2.2) in the EHAC/ACA sample.[40,46] Next, we subsequently irradiated the sample with visible (400-450nm) light. Figure 5.4C presents the visual evidence of the sample following subsequent visible light irradiation. The photographs show that the sample has been reverted back toward its original properties. The sample has been converted back to a thin, runny fluid that can be poured easily out of a tilted vial. Thus, Figure 5.4 demonstrates a dramatic and reversible light-induced rheological transition in the EHAC/ACA sample. Based on the spectra in Figure 5.3, the rheological change is clearly a result of the *trans* to *cis* and *cis* to *trans* photoisomerization of ACA.

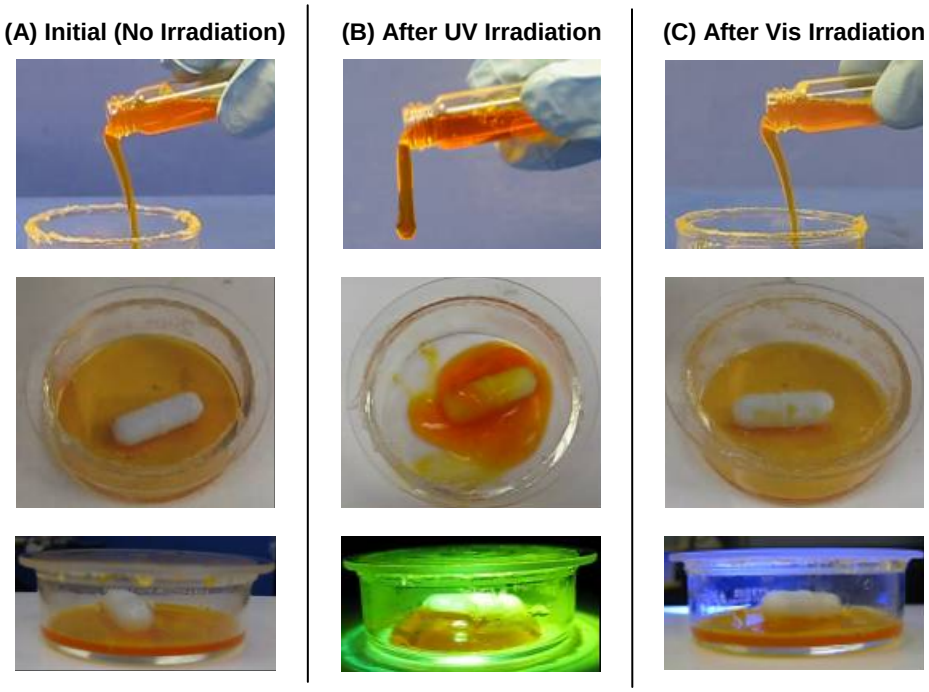

Figure 5.4. Photographs of a 40 mM EHAC 22 mM ACA (A) before, (B) after UV irradiation, and (C) after visible irradiation. (A) Initially, ACA is in its *trans* form and the sample has a low viscosity. Consequently, the sample flows rapidly out of a tilted vial (top) and bubbles are able to rise rapidly to the liquid surface. Also, the sample does not stick to the stir bar (bottom). (B) Upon UV irradiation, ACA is isomerizes to its *cis* form. In turn, the sample viscosity is significantly increased, as shown the sample does not flow easily out of a tilted vial (top) and retains bubbles for a long time. Moreover, the sample sticks to the stir bar when stirred (bottom). (C) Upon irradiation with visible light, ACA is isomerized back to its *trans* form. Consequently, the sample reverts back to a low viscosity, runny fluid that flows easily out of a tilted vial (top).

The above visual observations can be quantified through rheological measurements. We ran steady-shear rheology on a sample containing 40 mM EHAC and 20 mM ACA. Figure 5.5 presents the steady-shear rheological measurements of the sample before irradiation, following UV irradiation for 1 hr, and following subsequent visible irradiation. Before any irradiation, the sample has a low viscosity (9 E^{-3} Pa·s) that is nearly independent of shear rate, indicating Newtonian behavior. Upon irradiation with UV light for 1 hr, the sample becomes non-Newtonian and shear-thinning, and the zero-

shear viscosity of the sample increases by 3 orders of magnitude (9 Pa·s). Following subsequent visible irradiation, the sample again shows a low viscosity (1 E^{-2} Pa·s) Newtonian behavior. Thus, the sheady-shear rheological data quantifies the reversible photorheological response of our EHAC/ACA samples.

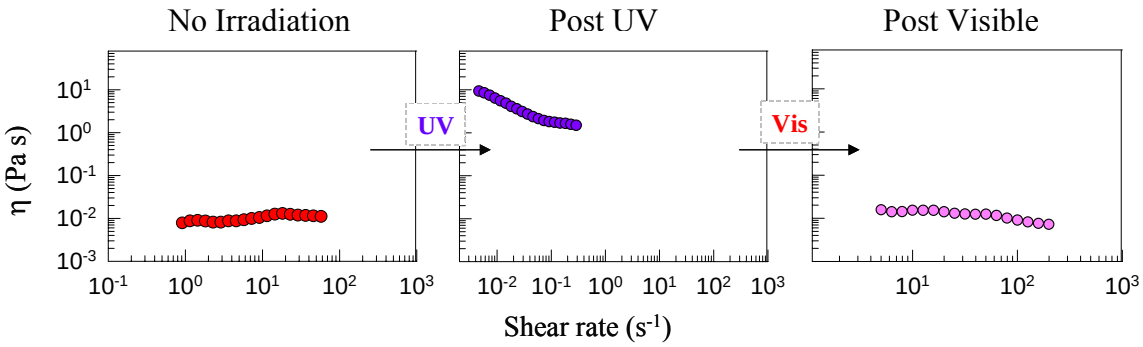

Figure 5.5 Steady-shear rheology of a 40 mM EHAC / 20 mM ACA sample in water. The sample transforms from a low viscosity Newtonian fluid, to a highly viscous shear-thinning fluid with UV irradiation. Subsequently, the sample transforms back to a low viscosity Newtonian fluid with visible irradiation.

Finally, we would like to discuss why the two photoisomers have differing effects on the EHAC micelles. We hope to rationalize these differing effect based on our knowledge of wormlike micelles and their self-assembly. As in chapter 3, we believe that there are two related factors to consider: (i) **the geometry** of the ACA isomers, and (ii) **their hydrophobicities**. Both these factors will influence the binding of ACA with EHAC micelles.

The first argument concerns the geometry of the ACA isomers. As discussed in Section 2.2, the key requirement for micellar growth is the binding (adsorption) of ACA counterions at the micellar interface.[40] ACA is expected to adsorb in such a way that the

azobenzene group is embedded in the hydrophobic interior of the micelle, while the carboxylate anion is located next to the cationic headgroups at the surface.[46,48] Such an orientation is possible for *trans*-ACA but more difficult for *cis*-ACA (Figure 5.1). In the case of *cis*-ACA, the carboxylate group becomes oriented on the same side of the benzene ring making it difficult for the former to orient inward and the latter outward relative to the micellar interface. Therefore, the geometric arguments suggest that *trans*-ACA can strongly associate with EHAC micelles, whereas *cis*-ACA will associate weakly.

A second related argument concerns the relative hydrophobicities of the two isomers: specifically, we believe that *trans*-ACA is more hydrophobic than *cis*-ACA. As previously mentioned in chapter 3, greater hydrophobicity of the *trans* isomer has been noted for a variety of azobenzene compounds.[8,9] Therefore, the hydrophobicity arguments support the geometric reasoning discussed above.

Ultimately these arguments lead to a mechanism that is similar to that in chapter 3. When *trans*-ACA is mixed with EHAC, the counterions will strongly bind to EHAC micelles, causing growth of worms followed by a decrease to short cylindrical micelles with additional *trans*-ACA. Upon UV irradiation, *trans*-ACA is converted to *cis*-OMCA, which has a much weaker interaction with EHAC, and will therefore tend to desorb from the micellar interface. As a result, causing an increase in the worms' length, thereby, driving a sharp increase in the solution viscosity. Upon subsequent irradiation with visible light, cis-ACA is converted back to *trans*-ACA, causing the solution to recover its

original properties. The above hypothesis, although somewhat speculative, promises to tie together the observed rheological changes with light. More studies need to be run before a complete argument can be hypothesized, this is discussed in the future recommendations section 6.2.1.

5.4 Conclusions

We have demonstrated reversible, light-tunable rheological properties in a micellar fluid consisting of the cationic surfactant, EHAC, and the photoresponsive molecule, ACA. When ACA is in its *trans* form, it's mixture with EHAC gives rise to a low viscosity, Newtonian fluid. Upon irradiation by UV light, *trans*-ACA is isomerized to *cis*-ACA. Consequently, the *cis* isomer gives rise to a highly viscoelastic fluid. Upon irradiation with visible light, the *cis*-ACA isomerizes back to *trans*-ACA, causing the sample to revert back to its original properties. An increase in zero-shear viscosity by several orders of magnitude can be induced in these fluids upon UV light irradiation, followed by a drop in the viscosity with subsequent irradiation with visible light. Such fluids could thus be promising for use in microscale flow-control devices.

Chapter 6

Conclusions and Recommendations

6.1 Conclusions

Previous formulations of PR fluids required synthesis of complex photosensitive molecules, which hampered the widespread use of these fluids. In this dissertation, we have reported three new simple classes of PR fluids that require no special synthesis and can therefore be easily replicated in any laboratory from inexpensive chemicals. These consist of: (1) a one-way aqueous PR fluid (Chapter 3), a one-way PR fluid based on a non-polar organic solvent (Chapter 4), and a reversible aqueous PR fluid (Chapter 5). Such PR fluids may be useful in a variety of applications, such as in sensors and valves in microfluidic devices.

In the first study (Chapter 3), we demonstrated a one-way, light-induced viscosity reduction (photothinning) in a new class of aqueous micellar fluids. These fluids consisted of the cationic surfactant, CTAB, and an organic photoresponsive molecule, OMCA. When the *trans* form of OMCA was added to CTAB micelles, the solution became highly viscous and viscoelastic. Upon irradiation with UV light, *trans*-OMCA was photoisomerized to *cis*-OMCA, which caused the sample to transform into a low viscosity, Newtonian fluid. Using techniques such as SANS and UV-Vis spectroscopy,

we were able to show that the light-induced transitions at the molecular level correlated at the microstructural level with a reduction in the length of wormlike micelles.

In the second study (Chapter 4), we extended our studies to non-aqueous PR fluids consisting of reverse micelles. We showed how to formulate such PR fluids based on mixtures of lecithin and water along with a photoresponsive molecule, HNS. In this system, we demonstrated that UV light could induce one-way rheological transitions, with the viscosity either increasing or decreasing depending on the system composition. In particular, certain samples underwent photogelling, i.e., they were transformed from low-viscosity solutions to gel-like materials upon irradiation with UV light. Again, the origin of these changes was the photoisomerization of HNS at the molecular level, which was postulated to impact the interfacial activity of HNS.

Finally, our last study (Chapter 5) demonstrated a reversible rheological change in an aqueous micellar fluid. These fluids consisted of the cationic surfactant, EHAC, and the photoresponsive molecule, ACA. Certain mixtures of EHAC and ACA produced low viscosity, Newtonian fluids. Upon irradiation by UV light, the solutions became highly viscous and viscoelastic. When these solutions were subsequently irradiated with visible light, they reverted to their low viscosity state. Conceptually, this system was similar to that reported in Chapter 1, with the important difference that the ACA molecule could undergo both a trans-cis photoisomerization under UV light as well as a cis-trans isomerization under visible light.

6.2 Recommendations for Future Work

We suggest three feasible projects for future work, which would extend the studies conducted in this dissertation as well as explore new concepts and applications.

6.2.1 Refinement of Reversible PR Fluids

In Chapter 5, we have reported a new class of reversible aqueous PR fluids. As part of future work, this study can be extended and the system can be further refined and optimized. Dynamic and steady-shear rheological studies could be preformed to help quantify the observed visual observations. Solubility studies could be used to help confirm the hypothesis of the differing hydrophobicities of the two isomers. Also, SANS measurements would be very helpful in confirming the structural changes that occur on the nano-scale. Moreover, alternate additives similar to ACA should be considered for use in such systems – for example, other azobenzene or spiropyran derivatives. In particular, additives that can promote faster switching of rheological properties would be highly desirable.

6.2.2 Microfluidic Devices Incorporating PR Fluids

Our "smart" PR fluids offer the possibility of applications in microfluidic devices, as discussed in Chapter 1. These fluids are homogeneous, stable, single-phase solutions that assemble into structures at the nanoscale – thus, their intrinsic length scale is small enough for use in microfluidic devices. Also, the use of light as the stimulus allows for directed control at a precise spatial location (with a resolution on the order of microns).

We have begun some preliminary experiments on a microfluidic valve design with Prof. Donald DeVoe's research group using our first-generation PR fluid (CTAB/OMCA) described in Chapter 3. The idea is to simply block off a channel using a PR fluid in the gel state, and then using UV light to liquefy the PR fluid, thereby enabling flow in the channel. It is recommended that this collaboration be continued in future work. Also, the fluids with reversible, light induced changes in rheological properties (Chapter 5) could be especially interesting for such microfluidic applications.

6.2.3 Photo-Patterning of Aqueous Gels

Finally, we suggest a future project that is unrelated to viscosity switching, but could be interesting in its own way. This arose out of some initial experiments that we have conducted in our laboratory with spiropyran molecules. Spiropyrans are a class of photosensitive molecules that undergo a reversible color change when irradiated with different wavelengths of light. A number of researchers have been interested in these molecules as a means to create color-based sensors etc. The focus, in most cases, has been on derivatization of polymers or lipids with spiropyran moieties. In our work, we have focused on a commercially available spiropyran derivative, 6-nitro-BIPS (IUPAC name: 1',3',3'-trimethyl-6-nitrospiro[1-benzopyran-2,2-indoline]). This molecule is not soluble in water, but can be dissolved in small amounts in the presence of surfactant micelles. We added 6-nitro-BIPS to a viscoelastic, gel-like micellar fluid made from the cationic surfactant, CTAB and the organic salt, sodium salicylate (NaSal). As shown in Figure 6.1, the addition of the spiropyran to the gel-like material allows for the creation of colored patterns in the gel. To create a given pattern, a mask with this pattern was used

and UV light was passed through the mask and onto the gel (which is initially colorless). Upon irradiation, a pink-colored pattern is formed in the gel, corresponding to the regions of the mask that are exposed to the light. The pink color indicates the conversion of the spiropyran into its merocyanine form. Figure 6.1 shows that patterns over a size scale of millimeters can be formed in the gel. The pattern is maintained as long as the gel is stored in the dark – when exposed to visible light, the merocyanine reverts to its original spiropyran form and the pattern disappears. Future work on this project could involve the creation of patterns at smaller length scales as well as on other types of gels (e.g., gelatin gels containing surfactant). The key idea, again, is that no special synthesis of new molecules would be required – instead, these patternable materials can be created simply by mixing commercial spiropyrans with existing gel-forming molecules.

Figure 6.1. Patterning gels of CTAB/NaSal/spiropyran. UV light induces the pink-colored pattern, while visible light makes the pattern vanish. The patterns are formed by irradiating the gel through a mask corresponding to that pattern.

References

[1] Davies, T. Thermoreversible Transitions Between Self-Assembled Nanostructures in Aqueous Solution. Master of Science, University of Maryland, 2005.

[2] Larson, R. G. *The Structure and Rheology of Complex Fluids*; Oxford University Press: New York, 1998.

[3] Tung, S.-H. Self-Assembly of Amphiphilic Molecules in Organic Liquids Doctor of Philosophy, University of Maryland, 2007.

[4] Wolff, T.; Emming, C. S.; Suck, T. A.; Vonbunau, G. "Photorheological Effects in Micellar Solutions Containing Anthracene Derivatives. A Rheological and Static Low-Angle Light-Scattering Study." *Journal of Physical Chemistry* **1989**, *93*, 4894-4898.

[5] Hao, T. "Electrorheological fluids." *Advanced Materials* **2001**, *13*, 1847-1857.

[6] Rankin, P. J.; Ginder, J. M.; Klingenberg, D. J. "Electro- and magneto-rheology." *Current Opinion in Colloid and Interface Science* **1998**, *3*, 373-381.

[7] Eastoe, J.; Vesperinas, A. "Self-assembly of light-sensitive surfactants." *Soft Matter* **2005**, *1*, 338-347.

[8] Lee, C. T.; Smith, K. A.; Hatton, T. A. "Photoreversible viscosity changes and gelation in mixtures of hydrophobically modified polyelectrolytes and photosensitive surfactants." *Macromolecules* **2004**, *37*, 5397-5405.

[9] Sakai, H.; Orihara, Y.; Kodashima, H.; Matsumura, A.; Ohkubo, T.; Tsuchiya, K.; Abe, M. "Photoinduced reversible change of fluid viscosity." *Journal of the American Chemical Society* **2005**, *127*, 13454-13455.

[10] Pouliquen, G.; Tribet, C. "Light-triggered association of bovine serum albumin and azobenzene-modified poly(acrylic acid) in dilute and semidilute solutions." *Macromolecules* **2006**, *39*, 373-383.

[11] Israelachvili, J. N. *Intermolecular and Surface Forces*; Academic Press: New York, 1992.

[12] Hoffmann, H. "Fascinating Phenomena in Surfactant Chemistry." *Advances in Colloid and Interface Science* **1990**, *32*, 123-150.

[13] Israelachvili, J. N.; Mitchell, D. J.; Ninham, B. W. "Theory of Self-Assembly of Hydrocarbon Amphiphiles into Micelles and Bilayers." *Journal of the Chemical Society-Faraday Transactions II* **1976**, *72*, 1525-1568.

[14] Mitchell, D. J.; Ninham, B. W. "Micelles, Vesicles and Micro-Emulsions." *Journal of the Chemical Society-Faraday Transactions II* **1981**, *77*, 601-629.

[15] Cates, M. E.; Candau, S. J. "Statics and Dynamics of Worm-Like Surfactant Micelles." *Journal of Physics-Condensed Matter* **1990**, *2*, 6869-6892.

[16] Yang, J. "Viscoelastic wormlike micelles and their applications." *Current Opinion in Colloid and Interface Science* **2002**, *7*, 276-281.

[17] Hoffmann, H. Viscoelastic Surfactant Solutions. In *Structure and Flow in Surfactant Solutions*; Herb, C. A., Prud'homme, R. K., Eds. Washington D.C., 1994; Vol. 578; pp 2-31.

[18] Appell, J.; Porte, G. "Polymer-Like Behavior of Giant Micelles." *Europhysics Letters* **1990**, *12*, 185-190.

[19] Candau, S. J.; Hirsch, E.; Zana, R.; Adam, M. "Network Properties of Semidilute Aqueous Kbr Solutions of Cetyltrimethylammonium Bromide." *Journal of Colloid and Interface Science* **1988**, *122*, 430-440.

[20] Imae, T.; Ikeda, S. "Sphere Rod Transition of Micelles of Tetradecyltrimethylammonium Halides in Aqueous Sodium-Halide Solutions and Flexibility and Entanglement of Long Rodlike Micelles." *Journal of Physical Chemistry* **1986**, *90*, 5216-5223.

[21] Kern, F.; Lemarechal, P.; Candau, S. J.; Cates, M. E. "Rheological Properties of Semidilute and Concentrated Aqueous-Solutions of Cetyltrimethylammonium Bromide in the Presence of Potassium-Bromide." *Langmuir* **1992**, *8*, 437-440.

[22] Rehage, H.; Hoffmann, H. "Viscoelastic Surfactant Solutions - Model Systems for Rheological Research." *Molecular Physics* **1991**, *74*, 933-973.

[23] Harrison, W. J.; McDonald, M. P.; Tiddy, G. J. T. "Phase-Behavior and Mesophase Formation in the Lithium Phenylstearate + 1-Phenylheptane System." *Journal of Physical Chemistry* **1991**, *95*, 4136-4140.

[24] Hellweg, T.; Eimer, W. "The micro-structures formed by Ni2+-AOT/cyclohexane/water microemulsions: a light scattering study." *Colloids and Surfaces a-Physicochemical and Engineering Aspects* **1998**, *136*, 97-107.

[25] Scartazzini, R.; Luisi, P. L. "Organogels from Lecithins." *Journal of Physical Chemistry* **1988**, *92*, 829-833.

[26] Steytler, D. C.; Jenta, T. R.; Robinson, B. H.; Eastoe, J.; Heenan, R. K. "Structure of reversed micelles formed by metal salts of bis(ethylhexyl) phosphoric acid." *Langmuir* **1996**, *12*, 1483-1489.

[27] Yu, Z. J.; Neuman, R. D. "Giant Rodlike Reversed Micelles Formed by Sodium Bis(2-Ethylhexyl) Phosphate in N-Heptane." *Langmuir* **1994**, *10*, 2553-2558.

[28] Shchipunov, Y. A.; Shumilina, E. V. "Lecithin Bridging by Hydrogen-Bonds in the Organogel." *Materials Science and Engineering C-Biomimetic Materials Sensors and Systems* **1995**, *3*, 43-50.

[29] Willard, D. M.; Riter, R. E.; Levinger, N. E. "Dynamics of polar solvation in lecithin/water/cyclohexane reverse micelles." *Journal of the American Chemical Society* **1998**, *120*, 4151-4160.

[30] Saltiel, J.; Sears, D. F. J. K., Dong-Hoon ; Park, Kyung-Mi. Cis-Trans Isomerization of Alkenes. In *CRC Handbook of Organic Photochemistry and Photobiology*; Horspool, W. M., Song, P.-S., Eds.; CRC Press, Inc.: New York, 1995; Vol. 2.

[31] Rau, H. Photoisomerization of Azobenzenes. In *Photochemistry and Photophysics*; Rabek, J. F., Ed.; CRC Press: Boca Raton, Fl., 1990; Vol. 2.

[32] Suginome, H. E,Z-Isomerization of Imines, Oximes, and Azo Compounds. In *CRC Handbook of Organic Photochemistry and Photobiology*; Horspool, W. M., Song, P.-S., Eds.; CRC Press, Inc.: New York, 1995; pp 824-840.

[33] Mohan, J. *Organic Spectroscopy Principles and Applications, 2nd edition*; Alpha Science International Ltd.: India, 2004.

[34] Macosko, C. W. *Rheology: Principles, Measurements and Applications*; VCH Publishers: New York, 1994.

[35] Morrison, F. A. *Understanding Rheology*; Oxford University Press: New York, 2001.

[36] Zemb, T.; Lindner, P. *Neutron, X-Ray and Light Scattering: Introduction to an Investigative Tool for Colloidal and Polymeric Systems*; Elsevier: Amsterdam, 1991.

[37] Pedersen, J. S. "Analysis of small-angle scattering data from colloids and polymer solutions: modeling and least-squares fitting." *Advances in Colloid and Interface Science* **1997**, *70*, 171-210.

[38] Feigin, L. A.; Svergun, D. I. *Structure Analysis by Small-Angle X-Ray and Neutron Scattering*; Plenum Press: New York, 1987.

[39] Raghavan, S. R.; Kaler, E. W. "Highly viscoelastic wormlike micellar solutions formed by cationic surfactants with long unsaturated tails." *Langmuir* **2001**, *17*, 300-306.

[40] Berret, J. F. In *Molecular Gels*; Weiss, R. G., Terech, P., Eds.; Springer: Dordrecht, 2005; pp 235-275.

[41] Muller, N.; Wolff, T.; Vonbunau, G. "Light-Induced Viscosity Changes of Aqueous-Solutions Containing 9-Substituted Anthracenes Solubilized in Cetyltrimethylammonium Micelles." *Journal of Photochemistry* **1984**, *24*, 37-43.

[42] Wolff, T.; Klaussner, B. "Overlap of Colloid Chemistry and Photochemistry in Surfactant Systems." *Advances in Colloid and Interface Science* **1995**, *59*, 31-94.

[43] Yu, X. L.; Wolff, T. "Rheological and photorheological effects of 6-alkyl coumarins in aqueous micellar solutions." *Langmuir* **2003**, *19*, 9672-9679.

[44] Murata, K.; Aoki, M.; Suzuki, T.; Harada, T.; Kawabata, H.; Komori, T.; Ohseto, F.; Ueda, K.; Shinkai, S. "Thermal and Light Control of the Sol-Gel Phase-Transition in Cholesterol-Based Organic Gels - Novel Helical Aggregation Modes as Detected by Circular-Dichroism and Electron-Microscopic Observation." *Journal of the American Chemical Society* **1994**, *116*, 6664-6676.

[45] Imae, T.; Tsubota, T.; Okamura, H.; Mori, O.; Takagi, K.; Itoh, M.; Sawaki, Y. "Photocyclodimerization of Cinnamic Acid on a Reaction Matrix - Structural Effect of Molecular Assemblies Constructed by Amphiphilic Compounds." *Journal of Physical Chemistry* **1995**, *99*, 6046-6053.

[46] Davies, T. S.; Ketner, A. M.; Raghavan, S. R. "Self-assembly of surfactant vesicles that transform into viscoelastic wormlike micelles upon heating." *Journal of the American Chemical Society* **2006**, *128*, 6669-6675.

[47] Takagi, K.; Nakamura, T.; Katsu, H.; Itoh, M.; Sawaki, Y.; Imae, T. "Photochemical cyclodimerization of cinnmamic acids included in surfactant amine oxides." *Molecular Crystals and Liquid Crystals Science and Technology Section a-Molecular Crystals and Liquid Crystals* **1996**, *276*, A135-A138.

[48] Hassan, P. A.; Raghavan, S. R.; Kaler, E. W. "Microstructural changes in SDS micelles induced by hydrotropic salt." *Langmuir* **2002**, *18*, 2543-2548.

[49] Noyce, D. S.; King, P. A.; Kirby, F. R.; Reed, W. L. "Kinetics of Acid-Catalyzed Isomerization of Cis-Cinnamic Acid." *Journal of the American Chemical Society* **1962**, *84*, 1632-1635.

[50] Eastoe, J.; Sanchez-Dominguez, M.; Wyatt, P.; Heenan, R. K. "A photo-responsive organogel." *Chemical Communications* **2004**, 2608-2609.

[51] Luisi, P. L. S., R.; Haering, G.; Schurtenberger, P. "Organogels from Water-in-Oil Microemulsions." *Colloid and Polymer Science* **1990**, *268*, 356-374.

[52] Schurtenberger, P. M., L. J.; King, S. M.; Lindner, P. "Cylindrical Structure and Flexibility of Polymer-Like Lecithin Reverse Micelles." *Journal of Physical Chemistry* **1991**, *95*, 4173-4176.

[53] Schurtenberger, P. S., R.; Luisi, P.L. "Viscoelastic Properties of Polymer-Like Reverse Micelles." *Rheologica Acta* **1989**, *28*, 372-381.

[54] Schurtenberger, P. S., R.; Magid, L. J.; Leser, M. E.; Luisi, P. L. " Structural and Dynamic Properties of Polymer-Like Reverse Micelles." *Journal of Physical Chemistry* **1990**, *94*, 3695-3701.

[55] Shchipunov, Y. A. "Lecithin organogel - A micellar system with unique properties." *Colloids and Surfaces a-Physicochemical and Engineering Aspects* **2001**, *183*, 541-554.

[56] Aliotta, F. "Percolative phenomena and electrorheological structures in reverse micelles." *Journal of Physics-Condensed Matter* **2002**, *14*, 2453-2460.

[57] Aliotta, F.; Fazio, B. "Percolative phenomena in branched reverse micelles." *Physica a-Statistical Mechanics and Its Applications* **2002**, *304*, 111-118.

[58] Aliotta, F.; Fontanella, M. E.; Pieruccini, M.; Salvato, G.; Trusso, S.; Vasi, C.; Lechner, R. E. "Percolative phenomena in lecithin reverse micelles: the role of water." *Colloid and Polymer Science* **2002**, *280*, 193-202.

[59] Cirkel, P. A.; Fontana, M.; Koper, G. J. M. "Structure and percolation of inverted cylindrical branched micelles." *Journal of Dispersion Science and Technology* **2001**, *22*, 211-219.

[60] Shchipunov, Y. A.; Hoffmann, H. "Growth, branching, and local ordering of lecithin polymer-like micelles." *Langmuir* **1998**, *14*, 6350-6360.